Cryptic and Stereospecific Hydroxylation, Oxidation, and Reduction in Platensimycin and Platencin Biosynthesis

Liao-Bin Dong,[†,#] Xiao Zhang,[†,#] Jeffrey D. Rudolf,[†] Ming-Rong Deng,[†] Edward Kalkreuter,[†]

Alexis J. Cepeda,[†] Hans Renata,[†] and Ben Shen[,†,‡,§]*

[†]Department of Chemistry, [‡]Department of Molecular Medicine, and [§]Natural Products Library Initiative at The Scripps Research Institute, The Scripps Research Institute, Jupiter, Florida 33458, United States

[*]To whom correspondence should be addressed: The Scripps Research Institute, 130 Scripps Way, #3A1, Jupiter, FL 33458; Tel: (561) 228-2456, Email: shenb@scripps.edu

[#]These authors contributed equally.

Table of Contents

Supplementary Materials and Methods..... S3

Supplementary Tables..... S12
Table S1. Strains used in this study..... S12
Table S2. Plasmids and cosmids used in this study..... S12
Table S3. Primers used in this study..... S13
Table S4. Summary of NMR data for compounds **6** and **7**..... S14
Table S5. Summary of NMR data for compounds **10** and **11**..... S15

Supplementary Figures..... S16
Figure S1. The B-ring construction of gibberellins biosynthesis..... S16
Figure S2. Structures and proposed biosynthetic pathway of PTM and PTN and their thioacid analogs, thioPTM and thioPTN..... S17
Figures S3–S5. Southern analysis of mutants SB12045–SB12047..... S18
Figures S6–S9. ^{1}H and ^{13}C NMR spectra of **5** and **9**..... S20
Figure S10. SDS-PAGE gel and size-exclusion chromatography of PtmO3 and PtmO6..... S22
Figures S11–S18. ^{1}H, ^{13}C, and ROESY NMR spectra of **6** and **10**..... S22
Figure S19. Steady-state kinetics of PtmO3 and PtmO6..... S27
Figures S20–S25. ^{1}H and ^{13}C NMR spectra of chemical synthesis of **5** analogues..... S28
Figure 26. Homology modeling and docking of substrates in PtmO6..... S31
Figure 27. A proposed mechanism of stereoselective hydroxylation of PtmO6..... S33
Figures S28, S29. Southern analysis of mutants SB12048 and SB12049..... S34
Figures S30–S35. HRESIMS and ^{1}H and ^{13}C NMR spectra of **7** and **11**..... S35
Figure S36. SDS-PAGE gel and size-exclusion chromatography of PtmO8 and PtmO1..... S38
Figure S37. Steady-state kinetics of PtmO8 and PtmO1..... S39
Figure S38. Homology models of PtmO8 and PtmO1..... S40
Figure S39. A plausible biosynthetic pathway to the enone in PTM and PTN biosynthesis..... S41

Supporting References..... S42

Supplementary Materials and Methods

Bacterial strains, plasmids, and chemicals. Strains, plasmids, and PCR primers used in this study are listed in Tables S1-S3. PCR primers were obtained from Sigma-Aldrich. Q5 high-fidelity DNA polymerase, restriction endonucleases, and T4 DNA ligase were purchased from NEB and used by following the protocols provided by the manufacturers. DNA gel extraction and plasmid preparation kits were purchased from Omega Bio-Tek. DNA sequencing was conducted by Eton Bioscience. The REDIRECT Technology kit for PCR-targeting homologous recombination was provided by The John Innes Center (Norwich, U.K.).[1] *E. coli* ET12567/pUZ8002 was used as the host for intergeneric conjugations.[2] Cosmid libraries were screened by PCR using OneTaq 2X Master Mix with GC buffer (NEB). For Southern analysis, digoxigenin labeling of DNA probes, hybridization, and detection were performed according to the protocols provided by the manufacturer (Roche Diagnostics Corp.). *S. platensis* CB00739 and its pathway-specific negative regulator *ptmR1* inactivation mutants, SB12029, were reported previously.[3] Other common chemicals, biochemical, and media components were purchased from standard commercial sources.

General experimental procedures. All ^{1}H, ^{13}C, and 2D NMR (^{1}H-^{1}H COSY, ^{1}H-^{13}C HSQC, ^{1}H-^{13}C HMBC, ^{1}H-^{1}H ROESY) experiments were run on a Bruker Avance III Ultrashield 700 MHz with QCI Cryoprobe or a Bruker AVANCE NEO 600 MHz with TCI Cryoprobe. Preparative HPLC was carried out on an Agilent 1260 Infinity LC equipped with an Agilent Eclipse XDB-C18 column (250 mm × 21.2 mm, 7 μm). LC-MS was performed on an Agilent 1260 Infinity LC coupled to a 6230 TOF (HRESI) equipped with an Agilent Poroshell 120 EC-C18 column (50 mm × 4.6 mm, 2.7 μm). Optical rotations were obtained using an AUTOPOL IV automatic polarimeter (Rudolph Research Analytical). IR spectra were attained using a Spectrum One FT-IR spectrophotometer (PerkinElmer). X-ray crystallographic data were obtained on a Bruker AXS Smart APEX CCD diffractometer using graphite monochromated MoKα radiation. The crystal structure was solved by direct methods (SHELXS97)[4] and refined by least-squares calculations. The nonhydrogen atoms were refined anisotropically, and the hydrogen atoms were fixed at calculated positions.

Culture conditions. *E. coli* strains harboring plasmids or cosmids were grown in lysogeny broth (LB) with appropriate antibiotic selection. *Streptomyces* strains were grown on solid ISP4 or MS media at 28 °C or cultured in liquid tryptic soy broth (TSB) at 28 °C and 250 rpm, with appropriate antibiotic selection, if needed. *E. coli-Streptomyces* conjugations were plated onto ISP4 or MS media supplemented with 10 mM $MgCl_2$. Fermentation of *S. platensis* recombinant strains were conducted as described previously.[3] Briefly, fresh spores of *Streptomyces* strains were inoculated into TSB seed medium and cultured for 2 days. PTM fermentation medium was inoculated with 4% (v/v) seed culture and 3% (w/v) Amberlite XAD-16 resin (Sigma-Aldrich) and incubated at 28 °C and 250 rpm for 7 days.

Extraction and LC-MS analysis. Extraction of resin from small-scale fermentations followed previously reported protocols.[3] After fermentation of the recombinant *Streptomyces* strains, the resin was harvested by centrifugation, washed three times with H_2O, and extracted three times with CH_3OH. Liquid chromatography for LC-MS analysis was performed using an 18 min solvent gradient (0.4 mL min^{-1}) from 5% – 100% CH_3OH in H_2O containing 0.1% formic acid.

Individual inactivation of *ptmO3* in *S. platensis* SB12029 to afford the Δ*ptmR1*/Δ*ptmO3* mutant SB12045. The *ptmO3* gene was replaced with the *aac(3)IV* + *oriT* cassette from pIJ773 using λRED-mediated PCR-targeting mutagenesis[1] in *E. coli* BW25113/pIJ790 harboring pBS12064, a cosmid containing the 5'-end of the *ptm* gene cluster.[5] The genotype of the resultant Δ*ptmO3* mutant cosmid, pBS12100, was confirmed by PCR analysis using primers 739O3ID_F and 739O3ID_R (Table S3). pBS12100 was transformed into *E. coli* ET12567/pUZ8002 and introduced into *S. platensis* SB12029 by intergeneric conjugation. Single crossovers of *ΔptmR1/ΔptmO3* were selected by screening for apramycin resistance on ISP4 medium. After another round of passaging the single-crossover exconjugants in solid ISP4 medium, the *ΔptmR1/ΔptmO3* mutant SB12045, a result of double-crossover homologous recombination, was selected for by screening for an apramycin resistant and kanamycin sensitive phenotype. The genotype of SB12045 was confirmed by Southern analysis (Figure S3).

Inactivation of *ptmO6* was performed using the protocol described above for the Δ*ptmR1*/Δ*ptmO3* mutant SB12045 to afford mutant SB12046. The genotype was verified by Southern analysis (Figures S4).

Inactivation of *ptmO3* and *ptmO6* in *S. platensis* SB12029 to afford the Δ*ptmR1*/Δ*ptmO3*/Δ*ptmO6* mutant SB12047. To construct an in-frame and markerless Δ*ptmO6* cosmid, pBS12101, a cosmid containing a partial *ptm* gene cluster with a Δ*ptmO6::aac(3)IV* gene disruption, was subjected to FLP-mediated cassette excision by its introduction into *E. coli* DH5α/BT340.[6] Following reported procedures,[1] overnight incubation at 42 °C resulted in loss of the *aac(3)IV* cassette and generation of an 81 bp scar, affording pBS12102. The *ptmO3* gene was then replaced with the *aac(3)IV* + *oriT* cassette from pIJ773 using λRED-mediated PCR-targeting mutagenesis in *E. coli* BW25113/pIJ790 harboring pBS12102. The genotype of the resultant Δ*ptmO3/*Δ*ptmO6* (makerless) mutant cosmid, pBS12103, was confirmed by PCR analysis using primers 739O3ID_F and 739O3ID_R together with 739O6ID_F and 739O6ID_R (Table S3). pBS12103 was transformed into *E. coli* ET12567/pUZ8002 and introduced into *S. platensis* SB12029 by intergeneric conjugation. Single crossovers of *ΔptmR1/*Δ*ptmO3/*Δ*ptmO6* were selected by screening for apramycin resistance on ISP4 medium. After several rounds of passaging the single-crossover exconjugants in solid ISP4 medium, the *ΔptmR1/*Δ*ptmO3/*Δ*ptmO6* mutant SB12047, a result of double-crossover homologous recombination, was selected for by screening for an apramycin resistant and kanamycin sensitive phenotype. The genotype of SB12047 was confirmed by Southern analysis (Figure S5).

Isolation and structural elucidation of (11*S*,16*S*)-*ent*-kauran-11,16-epoxy-19-oic acid (5) and *ent*-atiser-16-en-19-oic acid (9). A large-scale fermentation (6.0 L) of SB12047 was conducted in twelve 2.0 L baffled flasks, each containing 500 mL of production medium with 4% (v/v) seed culture. After incubation at 28 °C and 250 rpm for 7 days, the fermentation cultures were combined and extracted using hexane for three times. The combined hexane was dried using anhydrous Na_2SO_4 and removed in vacuo. The resulting oil was fractionated by silica gel column chromatography using a gradient elution system of hexane-EtOAc (0:1 to 1:0) to afford twelve fractions (Fr01-Fr12). The ^{1}H NMR spectra showed that Fr04 majorly contained *ent*-atiser-16-en-19-oic acid (**9**), which was then purified again by preparative reverse-phase HPLC using a 35 min elution system of 65–95% CH_3CN in H_2O containing 0.1% formic acid at a flow rate of 17 mL

min^{-1}. The fractions containing **9** (t_R = 30.5 min) were pooled. The solvent was removed in vacuo to yield 25 mg of **9** (white powder). The major constituent of Fr07 is (11*S*,16*S*)-*ent*-kauran-11,16-epoxy-19-oic acid (**5**), which was re-desolved in MeOH and sit at room temperature for two days to afford the crystals of **5** (colorless needles, >200 mg).

(11*S*,16*S*)-*ent*-Kauran-11,16-epoxy-19-oic acid (5). White, colorless needles (CH_3OH); mp 246.2–249.9 °C; ^{1}H NMR (700 MHz, pyridine-d_5): δ_H = 4.46 (br s, 1H), 2.50 (br d, 1H), 2.19 (m, 1H), 2.12 (t, *J* = 7.0 Hz, 1H), 2.07 (m, 1H), 2.05 (m, 1H), 1.94 (d, *J* = 11.2 Hz, 1H), 1.91 (dd, *J* = 11.9, 3.5 Hz, 1H), 1.88 (m, 1H), 1.77 (br d, *J* = 12.6 Hz, 1H), 1.66 (dd, *J* = 11.2, 3.5 Hz, 1H), 1.60 (br s, 1H), 1.47 (m, 1H), 1.45 (m, 2H), 1.42 (s, 3H), 1.36 (s, 3H), 1.34 (m, 1H), 1.17 (s, 3H), 1.16 (m, 1H), 1.10-1.03 (m, 3H) ppm; ^{13}C NMR (175 MHz, pyridine-d_5): δ_C = 180.6 (C), 85.8 (C), 77.1 (CH), 59.1 (CH), 57.8 (CH), 57.7 (CH_2), 46.3 (CH), 45.6 (C), 44.1 (C), 43.9 (CH_2), 42.1 (CH_2), 41.1 (CH_2), 39.0 (CH_2), 38.9 (CH_2), 37.7 (C), 29.8 (CH_3), 24.0 (CH_3), 22.7 (CH_2), 20.1 (CH_2), 18.2 (CH_3) ppm; The NMR data matched the literature.[3,5,7] HRESIMS affording $[M - H]^-$ ion at *m/z* 317.2141 (calcd $[M - H]^-$ for $C_{20}H_{29}O_3$ at *m/z* 317.2122). Crystallographic data for **5** was deposited in the Cambridge Crystallographic Data Centre (deposition number: CCDC 1894472).

***ent*-Atiser-16-en-19-oic acid (9).** White, amorphous solid; ^{1}H NMR (700 MHz, $CDCl_3$): δ_H = 4.73 (d, *J* = 2.1 Hz, 1H), 4.57 (d, *J* = 1.4 Hz, 1H), 2.23 (br s, 1H), 2.16 (br d, *J* = 14.0 Hz, 1H), 2.04 (br d, *J* = 16.8 Hz, 1H), 1.97 (br d, *J* = 11.9 Hz, 1H), 1.90-1.76 (m, 5H), 1.74 (s, 1H), 1.59 (m, 3H), 1.55 (m, 2H), 1.47 (dt, *J* = 13.3, 3.5 Hz, 1H), 1.40 (m, 3H), 1.25 (m, 1H), 1.24 (s, 3H), 1.14-0.97 (m, 6H), 0.90 (s, 3H), 0.85 (m, 2H) ppm; ^{13}C NMR (175 MHz, $CDCl_3$): δ_C = 183.3 (C), 152.8 (C), 104.5 (CH_2), 57.0 (CH), 52.1 (CH), 48.1 (CH_2), 43.7 (C), 39.6 (CH_2), 39.5 (CH_2), 38.3 (C), 37.9 (CH_2), 36.5 (CH), 33.4 (C), 28.9 (CH_3), 28.6 (CH_2), 28.2 (CH_2), 27.2 (CH_2), 20.2 (CH_2), 18.7 (CH_2), 12.0 (CH_3) ppm; The NMR data matched the literature.[8] HRESIMS affording $[M - H]^-$ ion at *m/z* 301.2196 (calcd $[M - H]^-$ for $C_{20}H_{29}O_2$ at *m/z* 301.2173).

Chemical synthesis of *ent*-atiser-16-en-19-oic acid (9). A reported five-step organic synthesis protocol from (–)-steviol to **9** was conducted to provide 5 mg of **9** with a total yield of 39%.[8] The ^{1}H NMR spectroscopic data was consistent with that in the literature.[8]

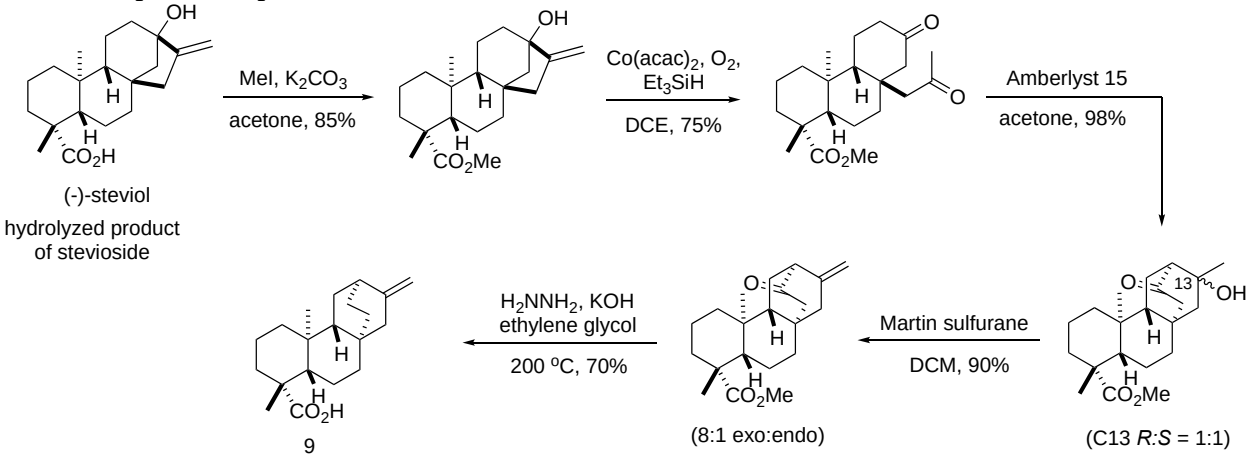

Scheme S1

Gene cloning. The PtmO3, PtmO6, PtmO8, and PtmO1 genes from *S. platensis* CB00739 were amplified by PCR from genomic DNA with Q5 DNA polymerase (NEB). The PCR product was

purified, treated with T4 polymerase, and cloned into pBS3080 according to ligation-independent procedures[9] to afford pBS12105 (harboring *ptmO3*), pBS12106 (harboring *ptmO6*), pBS12107 (harboring *ptmO8*), and pBS12108 (harboring *ptmO1*).

Gene expression and protein production and purification of PtmO3, PtmO6, PtmO8, and PtmO1 in *E. coli*. For enzyme activity assays, the plasmid harboring each gene was transformed into *E. coli* BL21(DE3) (Life Technologies) and grown in 1 or 2 liters of lysogeny broth (LB) at 37 °C with shaking at 250 rpm until an OD_{600} of 0.6 was reached. The culture was cooled to 4 °C, gene expression was induced with the addition of 0.25 mM isopropyl β-D-1-thiogalactopyranoside (IPTG), and the cells were grown around 18 h at 18 °C with shaking. After harvesting the cells by centrifugation at 4000 *g* for 30 min at 4 °C, the pellet was resuspended in lysis buffer (50 mM Tris, pH 8.0, containing 300 mM NaCl and 10 mM imidazole), lysed by sonication, and centrifuged at 15,000 *g* for 30 min at 4 °C. The supernatant was purified in two steps using an ÄKTA FPLC system (GE Healthcare Biosciences): a) nickel-affinity chromatography equipped with a HisTrap HP, 5 mL column (GE Healthcare Life Sciences), which was first washed with 100 mL Wash buffer (50 mM Tris, pH 8.0, containing 300 mM NaCl and 20 mM imidazole) and then eluted with a gradient increasing the concentration (0–50%, 120 mL) of Elution buffer (50 mM Tris, pH 8.0, containing 100 mM NaCl and 500 mM imidazole); b) anion exchange chromatography equipped with a HiTrap Q HP, 5 mL column (GE Healthcare Life Sciences) using a gradient increasing the concentration of sodium chloride from 0 to 1 M (250 ml) in 50 mM Tris, pH 8.0. The resultant protein with an N-terminal His_6-tag was concentrated and buffer switched to 50 mM Tris, pH 7.8, containing 100 mM NaCl, 50 mM KCl, and 5% glycerol, using an Amicon Ultra-15 concentrator (Millipore). Protein concentrations were determined from the absorbance at 280 nm using a molar absorptivity constant (PtmO3 and PtmO6, ε_{280} = 42,420 M^{-1} cm^{-1}; PtmO8, ε_{280} = 12,330 M^{-1} cm^{-1}; PtmO1, ε_{280} = 14,770 M^{-1} cm^{-1}). Individual aliquots of each protein were stored at –80 °C until use.

Analytical size-exclusion chromatography. The molecular weights (MW) and quaternary state of PtmO3, PtmO6, PtmO8, and PtmO1, respectively, in solution were determined by size-exclusion chromatography using a Superdex 200 16/600 column (GE Healthcare Life Sciences) connected to an ÄKTAxpress system (GE Healthcare LifeSciences). The column was pre-equilibrated with two column volumes of 50 mM Tris buffer, pH 8.0, and calibrated with ribonuclease A (13.7 kDa), carbonic anhydrase (29 kDa), ovalbumin (44 kDa), conalbumin (75 kDa), aldolase (158 kDa), and ferritin (440 kDa). The chromatography was carried out at 4 °C at a flow rate of 1 mL min^{-1}. The calibration curve of K_{av} versus log(MW) was prepared using the equation $K_{av} = (V_e - V_o) / (V_t - V_o)$, where V_e, V_o, and V_t is the elution volume, column void volume, and total bed volume, respectively.

Enzymatic activity of PtmO3 and PtmO6. Enzymatic reactions were performed in 50 mM Tris, pH 7.5, containing 200 μM $FeSO_4$ $7H_2O$, 2 mM α-ketoglutarate (α-KG), 1 mM ascorbic acid, 400 μM of **5** or **9**, and 2 μM of PtmO3 or PtmO6 in a total volume of 50 μL. After incubation at 30 °C for 10 min, 50 μL of CH_3OH were added to quench the reactions. The reaction mixture was then centrifuged and 5 μL of the supernatant were injected and analyzed by LC-MS. Liquid chromatography for LC-MS analysis was performed using an 18 min solvent gradient (0.4 mL min^{-1}) from 5% – 100% CH_3CN in H_2O containing 0.1% formic acid.

Kinetic studies of PtmO3 and PtmO6. Due to the inherent lack of significant UV absorption of these diterpenoids, PtmO3 and PtmO6 activities were measured by detecting succinate production with an adenosine triphosphate (ATP)-based luciferase assay (Succinate-Glo™ Assay, Promega, Madison, WI) according to manufacturers' instructions. This is a double-reagent-addition meGthod to rapidly detect succinate formation in Fe(II)/α-ketoglutarate-dependent dioxygenase reactions.[10] In brief, incubations were performed in 50 mM HEPES, pH 7.5, containing 10 μM $FeSO_4$ $7H_2O$, 10 μM α-KG, 100 μM ascorbic acid, and 20 nM of PtmO3 or PtmO6 with a total volume of 25 μL in 96-well plate. After incubation at room temperature for 10 min, 25μl of Succinate Detection Reagent I was added to each well of the 96-well plate to terminate the reaction. Gently mix 96-well plate with Vortex and incubate at room temperature for 60 minutes to fully convert succinate to ATP. Then, 50 μL of Succinate Detection Reagent II was added to each well of the 96-well plate and gently mixed using Vortex and incubated at room temperature for 30 minutes to generate light. The luminescence (RLU) was measured with a plate-reading luminometer (SpectraMax M5e, Molecular Devices) and converted into the amount of succinate formed uisng a standard curve. Each kinetic assay was performed in triplicate. The rates (k_{cat}) and Michaelis constants (K_m) were determined using a nonlinear fit of initial velocities versus substrate concentrations.

Chemical synthesis of the methyl ester of 5 (13) and a C19 *gem*-dimethyl analogue (14). (11*S*,16*S*)-*ent*-kauran-11,16-epoxy-19-oic acid (**5**) was isolated from a large-scaled fermentation of SB12047 in this study.

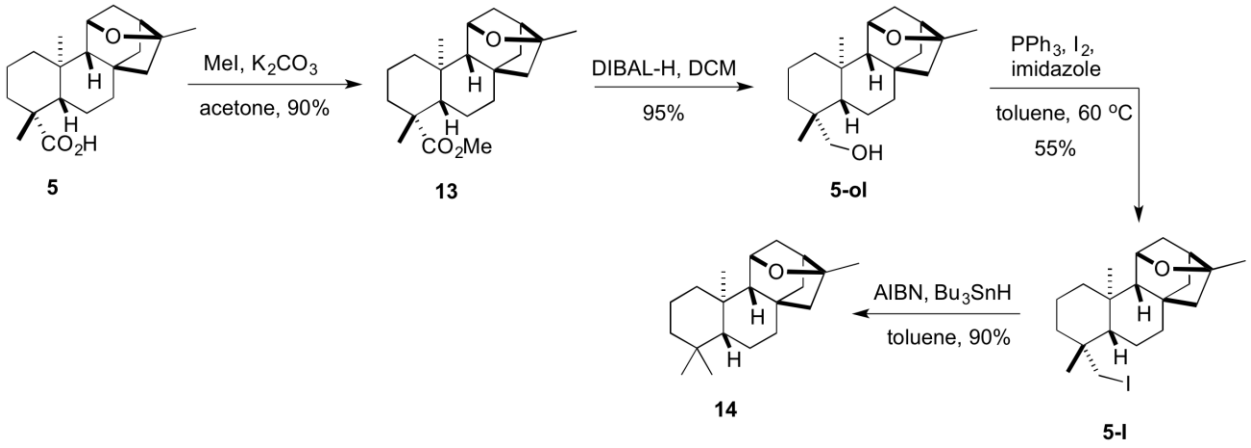

Scheme S2

Chemical synthesis of 13. To a mixture of **5** (200 mg, 0.629 mmol) and K_2CO_3 (260 mg, 1.89 mmol) in dry acetone was added iodomethane (0.08 mL, 1.26 mmol) in one portion. The reaction was stirred at 50 °C for five hours, then thin layer chromatography (TLC) showed complete consumption of the starting material. The mixture was filtered and concentrated, then purified through column chromatography to give **13** (189 mg, 0.568 mmol, 90.3%) as colorless oil. $[\alpha]_D^{25}$ –67.8 (c 0.50, CH_3OH); ^1H NMR (600 MHz, $CDCl_3$): δ_H = 4.35 (br t, *J* = 3.0 Hz, 1H), 3.63 (s, 3H), 2.20 (t, *J* = 6.6 Hz 1H), 2.19 (m, 1H), 2.00 (d, *J* = 10.8 Hz, 1H), 1.94 (dd, *J* = 11.4, 3.6 Hz, 1H), 1.88 (m, 1H), 1.83-1.78 (m, 2H), 1.76 (tt, *J* = 13.2, 4.2 Hz, 1H), 1.63 (m, 1H), 1.53 (dd, *J* = 10.8, 3.0 Hz, 1H), 1.50 (s, 1H), 1.46-1.41 (m, 3H), 1.34 (m, 1H), 1.34 (s, 3H), 1.24 (m, 1H), 1.17 (s, 3H), 1.11-1.00 (m, 3H), 0.86 (s, 3H) ppm; ^{13}C NMR (150 MHz, $CDCl_3$): δ_C = 178.1 (C), 85.6 (C), 76.9 (CH), 58.2 (CH), 57.4 (CH), 56.9 (CH_2), 51.2 (CH_3), 45.4 (CH), 45.0 (C), 43.6 (C), 43.4

(CH_2), 41.3 (CH_2), 40.5 (CH_2), 38.2 (CH_2), 38.0 (CH_2), 36.9 (C), 28.9 (CH_3), 23.2 (CH_3), 21.6 (CH_2), 19.0 (CH_2), 17.4 (CH_3) ppm. HRESIMS affording the $[M + H]^+$ ion at *m/z* 333.2422 (calcd $[M + H]^+$ for $C_{21}H_{33}O_3$ at 333.2424).

Chemical synthesis of 5-l. To a solution of **13** (100 mg, 0.30 mmol) in 10 mL dry dichloromethane at 0°C was added 1 M DIBAl-H in toluene (0.69 mL, 0.69 mmol) dropwisely. After stirring one hour, TLC showed complete consumption of the starting material. The reaction was quenched by adding 10 mL saturated aqueous seignette salt, and then allowed for stirring overnight. The mixture was extracted with dichloromethane, washed with brine, and then concentrated. The crude product was directly used for the next step without further purification.

To a stirred solution of **5-ol** (100 mg, 0.329 mmol), PPh_3 (112.2 mg, 0.427 mmol) and imidazole (44.8 mg, 0.658 mmol) in 10 mL dry toluene at 60°C was added I_2 (108.4 mg, 0.427mmol) in toluene dropwisely. The reaction was stirred for one hour, and then cooled to room temperature and concentrated. The crude residue was purified via flash column chromatography to give **5-l** (75 mg, 0.181 mmol, 55%) as colorless oil. $[\alpha]_D^{25}$ −14.6 (c 0.50, CH_3OH);^{1}H NMR (600 MHz, $CDCl_3$): δ_H = 4.32 (br s, 1H), 3.71 (d, *J* = 11.2 Hz 1H), 3.17 (dd, *J* = 11.2, 2.4 Hz 1H), 2.22 (t, *J* = 6.6 Hz 1H), 2.05 (d, *J* = 11.4 Hz 1H), 1.93-1.86 (m, 3H), 1.80 (m, 1H), 1.60 (s, 1H), 1.57-1.52 (m, 3H), 1.48 (m, 1H), 1.45-1.40 (m, 3H), 1.37 (d, *J* = 11.4 Hz, 1H), 1.34 (s, 3H), 1.31-1.28 (m, 2H), 1.23 (m, 1H), 1.09 (s, 3H), 1.11-1.05 (m, 3H), 1.03 (s, 3H) ppm; ^{13}C NMR (150 MHz, $CDCl_3$): δ_C = 85.5 (C), 76.7 (CH), 59.4 (CH), 57.1 (CH_2), 55.5 (CH), 45.5 (CH), 44.8 (C), 43.7 (CH_2), 40.8 (CH_2), 40.5 (CH_2), 38.7 (CH_2), 37.9 (CH_2), 36.9 (C), 36.6 (C), 33.3 (CH_3), 23.2 (CH_3), 20.1 (CH_2), 20.0 (CH_2), 19.2 (CH_3), 17.8 (CH_2) ppm. HRESIMS affording the $[M + H]^+$ ion at *m/z* 415.1507 (calcd $[M + H]^+$ for $C_{20}H_{32}IO$ at 415.1492).

Chemical synthesis of 14. To a solution of **5-I** (20 mg, 0.048 mmol) in dry toluene was added azobisisobutyronitrile (AIBN, 8.0 mg, 0.048 mmol) and Bu_3SnH (17 mg, 0.058 mmol), and then degassed and fulfilled with argon for three times. The reaction was stirred at 100 °C for one hour. TLC showed complete consumption of starting material. The reaction was concentrated and purified via flash column chromatography to afford **14** (12.5 mg, 0.043 mmol, 90%) as colorless oil. $[\alpha]_D^{25}$ −33.0 (c 0.50, CH_3OH); ^{1}H NMR (600 MHz, $CDCl_3$): δ_H = 4.34 (br t, *J* = 3.0 Hz, 1H), 2.20 (t, *J* = 6.6 Hz, 1H), 2.05 (d, *J* = 11.4 Hz, 1H), 1.98 (dd, *J* = 12.0, 3.6 Hz, 1H), 1.88 (m, 1H), 1.74 (m, 1H), 1.60-1.46 (m, 5H), 1.58 (s, 1H), 1.42-1.38 (m, 3H), 1.35 (d, *J* = 11.4 Hz, 1H), 1.34 (s, 3H), 1.30-1.20 (m, 2H), 1.16 (td, *J* = 13.2, 4.2 Hz, 1H), 1.08 (s, 3H), 1.03 (td, *J* = 13.2, 3.0 Hz, 1H), 0.86 (s, 3H), 0.84 (s, 3H), 0.80 (dd, *J* = 12.0, 1.8 Hz, 1H) ppm; ^{13}C NMR (150 MHz, $CDCl_3$): δ_C = 85.5 (C), 77.0 (CH), 59.2 (CH), 57.3 (CH_2), 56.5 (CH), 45.6 (CH), 44.9 (C), 43.9 (CH_2), 41.9 (CH_2), 41.0 (CH_2), 40.4 (CH_2), 37.9 (CH_2), 36.8 (C), 34.1 (CH_3), 33.1 (C), 23.3 (CH_3), 22.1 (CH_3), 20.0 (CH_2), 18.5 (CH_3), 18.4 (CH_2) ppm. HRESIMS affording the $[M + H]^+$ ion at *m/z* 289.2529 (calcd $[M + H]^+$ for $C_{20}H_{33}O$ at 289.2531).

Inactivation of *ptmR1* and *ptmO8* in *S. platensis* CB00739 to afford the Δ*ptmR1*/Δ*ptmO8* mutant SB12048. The *ptmR1* and *ptmO8* genes, which are adjacent to each other, were replaced with the *aac(3)IV* + *oriT* cassette from pIJ773 using λRED-mediated PCR-targeting mutagenesis in *E. coli* BW25113/pIJ790 harboring pBS12031, a cosmid containing the 3'-end of the *ptm* gene cluster.[11] The genotype of the resultant Δ*ptmR1*/Δ*ptmO8* mutant cosmid, pBS12104, was confirmed by PCR analysis using primers 739R1O8ID_F and 739R1O8ID_R (Table S3).

pBS12104 was transformed into *E. coli* ET12567/pUZ8002 and introduced into *S. platensis* CB00739 by intergeneric conjugation. Single crossovers of *ΔptmR1/ΔptmO8* were selected by screening for apramycin resistance on ISP4 medium. After another round of passaging the single-crossover exconjugants in solid ISP4 medium, the *ΔptmR1/ΔptmO8* mutant SB12048, a result of double-crossover homologous recombination, was selected for by screening for an apramycin resistant and kanamycin sensitive phenotype. The genotype of SB12048 was confirmed by Southern analysis (Figure S28).

Inactivation of *ptmO1* in *S. platensis* SB12029 to afford the Δ*ptmR1*/Δ*ptmO1* mutant SB12049. Inactivation of *ptmO1* was performed using the protocol described above for the Δ*ptmR1*/Δ*ptmO3* mutant SB12045 to afford mutant SB12049. The genotype was verified by Southern analysis (Figure S29).

Isolation and structural elucidation of (7*S*)-hydroxy-(11*S*,16*S*)-11,16-epoxy-*ent*-kauran-19-oic acid (6) and (7*S*)-7-hydroxy-*ent*-atiser-16-en-19-oic acid (10). A large-scale fermentation (4.0 L) of SB12048 was conducted in eight 2.0 L baffled flasks, each containing 500 mL of production medium with 4% (v/v) seed culture. After incubation at 28 °C and 250 rpm for 7 days, the fermentation cultures were combined and extracted using EtOAc for three times. The combined EtOAc was dried using anhydrous Na_2SO_4 and removed in vacuo. The resulting oil was fractionated by silica gel column chromatography using a gradient elution system of hexane-EtOAc (0:1 to 1:0) to afford fourteen fractions (Fr01-Fr14). The (7*S*)-hydroxy-(11*S*,16*S*)-11,16-epoxy-*ent*-kauran-19-oic acid (**6**, 150 mg) was isolated from Fr10. Fr06 was purified using preparative reverse-phase HPLC with a 30 min elution system of 30–68% CH_3CN in H_2O containing 0.1% formic acid at a flow rate of 17 mL min^{-1}. The fractions containing (7*S*)-7-hydroxy-*ent*-atiser-16-en-19-oic acid (**10**, t_R = 28.4 min) were pooled. The solvent was removed in vacuo to yield **10** (12 mg, white powder).

(7*S*)-Hydroxy-(11*S*,16*S*)-11,16-epoxy-*ent*-kauran-19-oic acid (6). Colorless cubes ($CH_3CN/CH_3COCH_3/H_2O$); mp 281.1–284.9 °C; $[\alpha]_D^{24}$ –43.3 (c 0.21, CH_3OH); IR (film) ν_{max} 2959, 1699, 1468, 1379, 1186, 1155, 1053, 1034, 970 cm^{-1}; ^1H NMR (700 MHz, DMSO-d_6): δ_H = 4.22 (br s, 1H), 3.29 (m, 1H), 2.15 (t, *J* = 6.3 Hz, 1H), 2.05 (d, *J* = 12.6 Hz, 1H), 1.97 (d, *J* = 11.9 Hz, 1H), 1.80–1.69 (m, 8H), 1.64 (br s, 1H), 1.34 (m, 1H), 1.26 (m, 1H), 1.25 (s, 3H), 1.21 (d, *J* = 10.5 Hz, 1H), 1.06 (s, 3H), 1.02 (td, *J* = 13.3, 4.2 Hz, 1H), 0.98 (td, *J* = 13.3, 4.2 Hz, 1H), 0.89 (s, 3H) ppm; ^{13}C NMR (175 MHz, DMSO-d_6): δ_C = 179.1 (C), 84.9 (C), 75.6 (CH), 72.4 (CH), 52.8 (CH), 52.4 (CH_2), 49.0 (C), 46.5 (CH), 45.0 (CH), 42.2 (C), 42.4 (CH_2), 41.0 (CH_2), 40.5 (CH_2), 37.7(CH_2), 36.4 (C), 29.4 (CH_2), 28.6 (CH_3), 23.3 (CH_3), 18.8 (CH_2), 17.3 (CH_3) ppm. The NMR data matched the literature.[12] For comparison, another set of NMR data of **6** in pyridine-d_5 is also reported (Table S4); HRESIMS affording the $[M - H]^-$ ion at *m/z* 333.2089 (calcd $[M - H]^-$ for $C_{20}H_{29}O_4$ at 333.2071). Crystallographic data for **6** was deposited in the Cambridge Crystallographic Data Centre (deposition number: CCDC 1877687).

(7*S*)-7-Hydroxy-*ent*-atiser-16-en-19-oic acid (10). White, amorphous solid; $[\alpha]_D^{24}$ –28.8 (c 0.17, CH_3OH); IR (film) ν_{max} 2928, 1689, 1469, 1138, 1043, 937, 874, 755 cm^{-1}; As the **10** was not previously characterized in full,[13] detailed spectroscopic characterization of **10** is reported here

(Table S5). HRESIMS affording the $[M - H]^-$ ion at *m/z* 317.2027 (calcd $[M - H]^-$ for $C_{20}H_{29}O_3$ at 317.2122).

Isolation and structural elucidation of 7-oxo-(11*S*,16*S*)-11,16-epoxy-*ent*-kauran-19-oic acid (7) and 7-oxo-*ent*-atiser-16-en-19-oic acid (11). A large-scale fermentation (4.0 L) of SB12049 was conducted in eight 2.0 L baffled flasks, each containing 500 mL of production medium with 4% (v/v) seed culture. After incubation at 28 °C and 250 rpm for 7 days, the fermentation cultures were combined and extracted using EtOAc for three times. The combined EtOAc was dried using anhydrous Na_2SO_4 and removed in vacuo. The resulting oil was fractionated by silica gel column chromatography using a gradient elution system of hexane-EtOAc (0:1 to 1:0) to afford ten fractions (Fr01-Fr10). Fr04 was purified using preparative reverse-phase HPLC with a 35 min elution system of 40–95% CH_3OH in H_2O containing 0.1% formic acid at a flow rate of 17 mL min^{-1}. The fractions containing 7-oxo-*ent*-atiser-16-en-19-oic acid (**11**, t_R = 33.8 min) were pooled. The solvent was removed in vacuo to yield **11** (8 mg, white powder). The 7-oxo-(11*S*,16*S*)-11,16-epoxy-*ent*-kauran-19-oic acid (**7**) was isolated from Fr06 by preparative reverse-phase HPLC with a 35 min elution system of 35–90% CH_3CN in H_2O containing 0.1% formic acid at a flow rate of 17 mL min^{-1}. The fractions containing **7** (t_R = 22.0 min) were pooled and the solvent of which was removed in vacuo to yield **7** (16 mg, white powder).

7-Oxo-(11*S*,16*S*)-11,16-epoxy-*ent*-kauran-19-oic acid (7). White, amorphous solid; $[\alpha]_D^{24}$ –33.9 (c 0.41, CH_3OH); IR (film) ν_{max} 2961, 2873, 1698, 1467, 1380, 1317, 1264, 1218, 1155, 1030 cm^{-1}; ^1H and ^{13}C NMR data, see Table S4; HRESIMS affording the $[M - H]^-$ ion at *m/z* 331.1911 (calcd $[M - H]^-$ for $C_{20}H_{27}O_4$ at 331.1915).

7-Oxo-*ent*-atiser-16-en-19-oic acid (11). White, amorphous solid; ^1H NMR (700 MHz, $CDCl_3$): δ_H = 4.76 (d, *J* = 2.1 Hz, 1H), 4.65 (d, *J* = 2.1 Hz, 1H), 3.12 (t, *J* = 15.4 Hz, 1H), 2.63 (dd, *J* = 15.4, 2.8 Hz, 2H), 2.29 (br s, 1H), 2.23 (br d, *J* = 14.0 Hz, 1H), 2.09 (br d, *J* = 17.5 Hz, 1H), 2.04 (m, 1H), 1.89 (m, 1H), 1.68 (br d, *J* = 13.3 Hz, 1H), 1.65-1.60 (m, 3H), 1.51-1.42 (m, 4H), 1.30 (m, 1H), 1.21 (s, 3H), 1.09 (s, 3H), 1.00 (td, *J* = 13.3, 4.2 Hz, 1H), 0.91 (td, *J* = 13.3, 4.2 Hz, 1H) ppm; ^{13}C NMR (175 MHz, $CDCl_3$): δ_C = 215.7 (C), 181.2 (C), 150.4 (C), 106.4 (CH_2), 54.2 (CH), 52.1 (CH), 47.7 (C), 43.9 (C), 40.1 (CH_2), 39.5 (CH_2), 38.6 (CH_2), 38.2 (C), 38.0 (CH_2), 36.1 (CH), 28.7 (CH_3), 28.5 (CH_2), 27.8 (CH_2), 26.3 (CH_2), 18.9 (CH_2), 12.2 (CH_3) ppm; The NMR data matched the literature.[14] As the OR and IR data of **11** was not previously characterized,[14] this set of physical data is reported here. $[\alpha]_D^{24}$ –35.2 (c 0.31, CH_3OH); IR (film) ν_{max} 2933, 2866, 1694, 1467, 1311, 1258, 1180, 877 cm^{-1}; For comparison, another set of NMR data of **11** in pyridine-d_5 is also reported (Table S5); HRESIMS affording the $[M - H]^-$ ion at *m/z* 315.1989 (calcd $[M - H]^-$ for $C_{20}H_{27}O_3$ at 315.1966).

Enzymatic activity of PtmO8. When NAD^+ (500 μM) was used as a cofactor, the reaction was incubated in 50 mM Tris, pH 7.0, containing 200 μM **6** or **10**, and 1 μM PtmO8 with a total volume of 50 μL. When $NADP^+$ (500 μM) was used as a cofactor, the enzyme concentration of PtmO8 was increased to 4 μM. Both reactions were incubated at 30 °C for 10 min and then quenched by adding 50 μL of MeOH. The reaction mixture was then centrifuged and 5 μL of the supernatant were injected and analyzed by LC-MS. Liquid chromatography for LC-MS analysis was performed using an 18 min solvent gradient (0.4 mL min^{-1}) from 5% – 100% CH_3CN in H_2O containing 0.1% formic acid.

Enzymatic activity of PtmO1. When NADPH (500 μM) was used as a cofactor, the reaction was incubated in 50 mM Tris, pH 7.0, containing either 200 μM **7** and 0.1 μM PtmO1 or 200 μM **11** and 0.5 μM PtmO1, with a a total volume of 50 μL. When NADH (500 μM) was used as a cofactor, the enzyme concentration of PtmO1 was increased to 10 μM for both substrates **7** and **11**. After incubation at 30 °C for 10 min, 50 μL of CH_3OH were added to quench the reactions. The reaction mixture was then centrifuged and 5 μL of the supernatant were injected and analyzed by LC-MS. Liquid chromatography for LC-MS analysis was performed using an 18 min solvent gradient (0.4 mL min^{-1}) from 5% – 100% CH_3CN in H_2O containing 0.1% formic acid.

Kinetic study of PtmO8. Kinetic analysis was performed using a microplate reader (SpectraMax M5e, Molecular Devices) to measure the formation of NADH or NADPH (λ = 340 nm). When determine the kinetic parameters with substrates **6** and **10**, saturating concentration (500 μM) of NAD+ was used. Assays were performed in 96-well plate in 50 mM Tris, pH 7.0, containing varying concentrations of substrates **6** and **10** and 200 μM PtmO8, with a total volume of 150 μL. After incubation at room temperature for 10 min, 150 μL of CH_3OH were added to quench the reactions. The UV absorption at λ = 340 nm was measured with a microplate reader and converted into the amount of NADH formed uisng a standard curve. The same method was used to determine the kinetic parameters with NADH and NADPH, in which the saturating concentration (200 μM) of **10** was used. Each kinetic assay was performed in triplicate.

Kinetic study of PtmO1. Kinetic analysis was performed using a microplate reader (SpectraMax M5e, Molecular Devices) to measure the consumption of NADPH (λ = 340 nm). When determine the kinetic parameters with substrates **7** and **11**, saturating concentration (200 μM) of NADPH was used. Assays were performed in 96-well plate in 50 mM Tris, pH 7.0, containing varying concentrations of substrates **7** and **11** and 20-40 nM PtmO1, with a total volume of 150 μL. After incubation at room temperature for 10 min, 150 μL of CH_3OH were added to quench the reactions. The UV absorption at λ = 340 nm was measured with a microplate reader and converted into the amount of NADPH comsumed uisng a standard curve. Each kinetic assay was performed in triplicate.

(7*R*)-7-Hydroxy-(11*S*,16*S*)-11,16-epoxy-*ent*-kauran-19-oic acid (8). Colorless needles (CH_3OH); mp 301.0–304.9 °C; Compound **8** was previously isolated from *S. platensis* SB120xx in our group and used as an authentic standard in this study;[5] HRESIMS affording the $[M - H]^-$ ion at *m/z* 333.2076 (calcd $[M - H]^-$ for $C_{20}H_{29}O_4$ at 333.2071). Crystallographic data for **8** was deposited in the Cambridge Crystallographic Data Centre (deposition number: CCDC 1877686).

(7*R*)-7-Hydroxy-*ent*-ati-16-en-19-oic acid, occidentalic acid (12). Compound **12** was previously isolated from *S. platensis* SB120xx in our group and used as an authentic standard in this study;[5] HRESIMS affording the $[M - H]^-$ ion at *m/z* 317.2176 (calcd $[M - H]^-$ for $C_{20}H_{29}O_3$ at 317.2122).

Modeling of PtmO6 and substrates. The amino acid sequence for PtmO6 was uploaded to the I-TASSER online server to construct a homology model.[15] The first model was selected due to the strong C-score of 1.31. The placement of α-KG and iron was predicted based on structural alignment of the PtmO6 homology model with several other α-KG-dependent enzyme crystal structures using UCSF Chimera.[16-18] The PDB files for the docked structures of **5** and **9** were

constructed and minimized in Chem3D (PerkinElmer Informatics). Docked conformations of the PtmO6 substrates were manually inspected, and the best predictions are shown in Figure S26.

One-pot reaction using a combination of PtmO3, PtmO8, and PtmO1. Enzymatic reactions were performed in 50 mM Tris, pH 7.0, containing 200 μM $FeSO_4$ $7H_2O$, 2 mM α-KG, 1 mM ascorbic acid, 1 mM NAD^+, 1 mM NADPH, 400 μM of **5** or **9**, and 2 μM each of PtmO3, PtmO8, and PtmO1 in a total volume of 500 μL. This reaction was incubated at 30 °C and 50 μL of each mixture was taken at time points of 4 min, 10 min, and 30 min, and 50 μL of CH_3OH was added to quench the reactions. The reaction mixture was then centrifuged and 5 μL of the supernatant were injected and analyzed by LC-MS. Liquid chromatography for LC-MS analysis was performed using an 18 min solvent gradient (0.4 mL min^{-1}) from 5% – 100% CH_3CN in H_2O containing 0.1% formic acid. This one-pot reaction was performed in triplicate.

Supplementary Tables

Table S1. Strains used in this study.

Strain	Genotype, Description	Source (Reference)
E. coli DH5α	*E. coli* host for general cloning	Life Technologies
E. coli BL21 (DE3)	*E. coli* host for protein expression	Life Technologies
E. coli BW25113/pIJ790	*E. coli* host for λRED-mediated PCR targeting	(1)
E. coli ET12567/pUZ8002	Methylation-deficient *E. coli* host for intergeneric conjugation	(2)
S. platensis CB00739	For cloning of *ptmO3*, *ptmO6*, *ptmO1*, and *ptmO8*	(10)
S. platensis SB12029	CB00739 Δ*ptmR1* (markerless)	(3)
S. platensis SB12045	SB12029 Δ*ptmO3::aac(3)IV*	This study
S. platensis SB12046	SB12029 Δ*ptmO6::aac(3)IV*	This study
S. platensis SB12047	SB12029 Δ*ptmO3::aac(3)IV*/Δ*ptmO6* (markerless)	This study
S. platensis SB12048	CB00739 Δ*ptmR1O8::aac(3)IV*	This study
S. platensis SB12049	SB12029 Δ*ptmO1::aac(3)IV*	This study

Table S2. Plasmids and cosmids used in this study.

Plasmid	Description	Source (Reference)
pIJ773	Plasmid containing the apramycin resistance cassette (*aac(3)IV+oriT*)	(1)
pBS12031	Cosmid 18H9 containing a partial *ptm* gene cluster	(10)
pBS12037	Cosmid 18H9 containing a partial *ptm* gene cluster and Δ*ptmR1* (markerless)	(3)
pBS12064	Cosmid 17E7 containing a partial *ptm* gene cluster	(4)
pBS12100	pBS12064 Δ*ptmO3::aac(3)IV*	This study
pBS12101	pBS12064 Δ*ptmO6::aac(3)IV*	This study
pBS12102	pBS12064 Δ*ptmO6* (markerless)	This study
pBS12103	pBS12064 Δ*ptmO3::aac(3)IV*/Δ*ptmO6* (markerless)	This study
pBS12104	pBS12031 Δ*ptmR1O8::aac(3)IV*	This study

pBS12105	pBS12064 Δ*ptmO1::aac(3)IV*	This study
pBS3080	pRSFDuet-1 derived plasmid containing a *Bsm*FI site for ligation-independent cloning (LIC) and encodes a TEV protease site after the N-terminal His_6-tag	(8)
pBS12105	pBS3080 harboring *ptmO3*; used for enzyme assays	This study
pBS12106	pBS3080 harboring *ptmO6*; used for enzyme assays	This study
pBS12107	pBS3080 harboring *ptmO8*; used for enzyme assays	This study
pBS12108	pBS3080 harboring *ptmO1*; used for enzyme assays	This study

Table S3. Primers used in this study.

Primer	Nucleotide Sequence (5'-3')	Function
739O3_F	AAAACCTCTATTTCCAGTCGGCTGGGCTGGTGTGGGAG	*ptmO3* amplification for pBS12105
739O3_R	TACTTACTTAAATGTTATTACGCGGTGGCCTTGTCCTC	*ptmO3* amplification for pBS12105
739O6_F	AAAACCTCTATTTCCAGTCGGCTGGGCTGGTGTGGGAG	*ptmO6* amplification for pBS12106
739O6_R	TACTTACTTAAATGTTACTACGCGGCGGTGTTCTGCTG	*ptmO6* amplification for pBS12106
739O8_F	AAAACCTCTATTTCCAGTCGGTGGGCAGGCTTGAGGGG	*ptmO8* amplification for pBS12107
739O8_R	TACTTACTTAAATGTTATCACGTCTCGGCCCTCCG	*ptmO8* amplification for pBS12107
739O1_F	AAAACCTCTATTTCCAGTCGACTTCCCACCAGCGTCTGG	*ptmO1* amplification for pBS12108
739O1_R	TACTTACTTAAATGTTATCAGTGCACGATCGTGCG	*ptmO1* amplification for pBS12108
739O3KO_F	GGCTGGCTGGTGGCTGGGCTGGTGTGGGAGCCGACGTCTATTCCGGGGATCCGTCGACC	PCR targeting for replacement of *ptmO3*
739O3KO_R	TGAAGAGCGTGCGCCTCATTACGCGGTGGCCTTGTCCTCTGTAGGCTGGAGCTGCTTC	PCR targeting for replacement of *ptmO3*
739O3IDKO_F	TCGCAACTGTTGTTGTCGTTC	PCR confirmation
739O3IDKO_R	GAAGAGCGTGCGCCTCATTA	PCR confirmation
739O3south_F	GAGACCGCCCGTGCCTACTA	Southern probe *O3*
739O3south_R	AGCAGGCTGATGCCCTTGTG	Southern probe *O3*
739O6KO_F	GGCTGGCTGGTGGCTGGGCTGGTGTGGGAGCCGACGTCTATTCCGGGGATCCGTCGACC	PCR targeting for replacement of *ptmO6*
739O6KO_R	CCGGCAGAAAGGTGTGCGACGGCGCGACGCGGTCTACGCTGTAGGCTGGAGCTGCTTC	PCR targeting for replacement of *ptmO6*
739O6IDKO_F	CGCACTGGGTCGCTAAATCA	PCR confirmation
739O6IDKO_R	CGGAAATCCGGCAGAAAGGT	PCR confirmation
739O6south_F	TCGACACCTTCGACAACCGC	Southern probe *ptmO6*
739O6south_R	CGCCCCATATGCCGAGTACG	Southern probe *ptmO6*
739R1O8KO_F	GAGGAGTTCCAGACGGGTATTGGCGCCGCTCGCATTCAAATTCCGGGGATCCGTCGACC	PCR targeting for replacement of *ptmR1and ptmO8*
739R1O8KO_R	GGCGGGCGAAGTCCGGGCCGCCGCTCACGTCTCGGCCCTTGTAGGCTGGAGCTGCTTC	PCR targeting for replacement of *ptmR1and ptmO8*
739R1O8IDKO_F	CGCCGATGCGTTCGGTAG	PCR confirmation
739R1O8IDKO_R	GTGTGGCGGGCGAAGT	PCR confirmation
739R1O8south_F	CCCTGGCTCGGTTCGGTC	Southern probe *ptmR1and ptmO8*
739R1O8south_R	GCAGTGGCCCTTGAGGTAGC	Southern probe *ptmR1and ptmO8*
739O1KO_F	CTGGCCGCCGACGGCGCCGACGTCGTCGTCACCGGGCGCATTCCGGGGATCCGTCGACC	PCR targeting for replacement of *ptmO1*
739O1KO_R	GTCGGCCAGCGCCACCACGGCCCGGCCGATGTCGTGCTCTGTAGGCTGGAGCTGCTTC	PCR targeting for replacement of *ptmO1*

739O1IDKO_F	CACCTGGCAGACCTTCTGG	PCR confirmation
739O1IDKO_R	GTACCGGGAAAGGTTCTGGG	PCR confirmation
739O1south_F	TGGTGGGAAGTCATGGAGTGG	Southern probe *ptmO1*
739O1south_R	TATAGTCCTTTGAGGGTGGTGGT	Southern probe *ptmO1*

Table S4. Summary of ^{1}H NMR (700 MHz) and ^{13}C NMR (175 MHz) data for compounds **6** and **7** in pyridine-d_5 (δ in ppm, *J* in Hz)[a]

	6		**7**	
No.	δ_C	δ_H	δ_C	δ_H
1a	42.2, CH_2	1.83, br d (12.6)	41.2, CH_2	1.79, br d (12.6)
1b		1.21, td (13.3, 4.2)		1.04, td (13.3, 4.2)
2a	20.2, CH_2	2.23, m	19.9, CH_2	2.16, m
2b		1.48, m		1.48, m
3a	39.1, CH_2	2.54, br d (13.3)	38.5, CH_2	2.46, br d (13.3)
3b		1.15, td (13.3, 4.2)		1.02, td (13.3, 4.2)
4	43.8, C		44.0, C	
5	48.1, CH	2.33, t (7.0)	54.2, CH	1.53, dd (14.0, 2.8)
6a	31.2, CH_2	2.47, 2H, overlapped	40.3, CH_2	3.42, dd (15.4, 14.0)
6b				2.99, dd (15.4, 2.8)
7	74.3, CH	3.84, br s	212.2, C	
8	50.6, C		57.4, C	
9	54.3, CH	2.28, br s	58.6, CH	1.91, overlapped
10	37.8, C		37.6, C	
11	77.2, CH	4.55, br s	76.5, CH	4.49, t (3.5)
12a	41.6, CH_2	2.05, d (11.2)	41.1, CH_2	1.99, d (11.9)
12b		1.94, m		1.92, overlapped
13	46.4, CH	2.20, t (6.3)	45.7, CH	2.20, t (6.3)
14a	43.4, CH_2	1.87, br d (11.9)	44.0, CH_2	2.03, dd (11.9, 3.5)
14b		1.36, dd (11.2, 6.3)		1.56, dd (11.9, 7.0)
15a	53.8, CH_2	2.45, dd (11.2, 3.5)	51.0, CH_2	2.30, d (11.2)
15b		1.56, d (11.2)		1.94, dd (11.9, 3.5)
16	86.0, C		86.3, C	
17	24.1, CH_3	1.46, s	23.7, CH_3	1.44, s
18	29.8, CH_3	1.43, s	29.0, CH_3	1.26, s
19	181.0, C		179.9, C	
20	18.4, CH_3	1.25, s	17.2, CH_3	1.29, s

[a] Assignments are based on 1D and 2D NMR experiments.

Table S5. Summary of ^{1}H NMR (700 MHz) and ^{13}C NMR (175 MHz) data for compounds **10** and **11** in pyridine-d_5 (δ in ppm, *J* in Hz)[a]

	10		**11**	
No.	δ_C	δ_H	δ_C	δ_H
1a	40.5, CH_2	1.64, overlapped	39.8, CH_2	1.62, br d (12.6)
1b		1.03, td (13.3, 4.2)		0.88, td (12.6, 3.5)
2a	20.0, CH_2	2.31, m	19.7, CH_2	2.22, m
2b		1.51, m		1.50, m
3a	39.3, CH_2	2.52, br d (12.6)	38.7, CH_2	2.47, br d (13.3)
3b		1.17, td (12.6, 2.8)		1.06, br t (12.6)
4	44.0, C		44.1, C	
5	48.5, CH	2.21, d (12.6)	54.2, CH	1.53, overlapped
6a	30.0, CH_2	2.62, td (13.3, 1.4)	39.4, CH_2	3.52, t (15.4)
6b		2.41, dt (14.0, 2.8)		2.96, dd (15.4, 3.5)
7	73.2, CH	3.78, br s	214.6, C	
8	39.1, C		48.0, C	
9	47.0, CH	1.93, dd (11.2, 5.6)	52.3, CH	1.50, overlapped
10	38.6, C		38.6, C	
11a	28.4, CH_2	1.64, overlapped	28.7, CH_2	1.59, m
11b		1.46, m		1.43, dd (11.9, 8.4)
12	37.5, CH	2.28, m	36.7, CH	2.26, m
13a	27.8, CH_2	1.64, overlapped	26.6, CH_2	1.53, 2H, m
13b		1.54, m		
14a	29.1, CH_2	1.89, br t (12.6)	28.2, CH_2	2.03, m
14b		1.10, m		1.31, td (12.6, 5.6)
15a	43.4, CH_2	3.00, dd (16.8. 2,8)	40.9, CH_2	2.90, dt (17.5. 2,8)
15b		2.18, d (16.1)		2.34, br d (17.5)
16	153.7, C		151.1, C	
17a	105.4, CH_2	4.92, d (2.8)	106.9, CH_2	4.91, d (2.1)
17b		4.78, d (2.1)		4.80, d (2.1)
18	29.6, CH_3	1.43, s	28.9, CH_3	1.28, s
19	180.9, C		179.9, C	
20	12.5, CH_3	1.20, s	12.5, CH_3	1.24, s

[a] Assignments are based on 1D and 2D NMR experiments.

Supplementary Figures

Figure S1. C7 β-hydroxylation as an essential early biosynthetic step in the B-ring construction of gibberellins biosynthesis. (A) B-ring construction of gibberellins biosynthesis in rhizobia.[19,20] CYP114 requires a ferredoxin (Fd_{GA}) for a full B-ring contraction reaction and shows low catalytic efficiency in converting GA_{12}-aldehyde to GA_{12}. The mechanism of B-ring contraction was confirmed via a semipinacol rearrangement. (B) B-ring construction in gibberellins biosynthesis in a plant-associated fungus, *Gibberella fujikuroi*.[21] The P450-1 not only catalyzes a three-step B-ring contraction but also hydroxylates C3 to form GA_{14}. (C) B-ring construction in gibberellins biosynthesis in plant, *Arabidopsis thaliana*.[22] The three-step reaction is identical to that found in rhizobia.

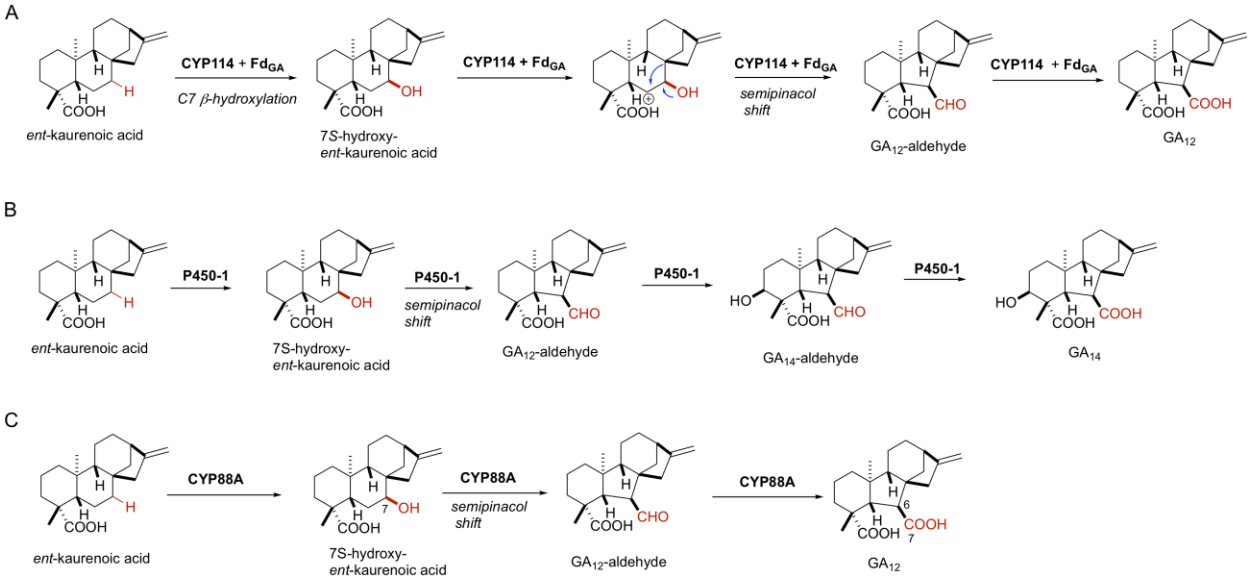

Figure S2. Structures and proposed biosynthetic pathway of PTM and PTN and their thioacid analogs, thioPTM and thioPTN. (A) Structures of PTM, PTN, thioPTM, and thioPTN. The aliphatic ketolide and 3-amino-2,4-dihydroxybenzoic acid (ADHBA) moieties are highlighted in blue and red, respectively. (B) The early steps of PTM biosynthesis are shown with isolated intermediates and the recombinant strains that produced each compound listed.[3,5,23,24] Ether formation occurs after oxidation of C19 and prior to C7 hydroxylation. After platensicyl-CoA is formed, PtmC catalyzes the coupling of ADHBA or ADHBSH to form PTM or thioPTM. (C) The early steps of PTN biosynthesis are shown with isolated intermediates and the recombinant strains that produced each compound listed.[3,5,23,24] The biosynthesis of PTN from *ent*-CPP parallels PTM with the exception of the PtmT1-catalyzed formation of *ent*-atiserene, which undergoes similar oxidations except for PtmO5, to afford platencinyl-CoA, which is coupled with ADHBA or ADHBSH to form PTN or thioPTN. The platencin SL4 was discovered by heterologous expression of the *ptn* biosynthetic gene cluster in *Streptomyces lividans* K4-114.[25] The enzymes characterized in this study are highlighted in red in both (B) and (C).

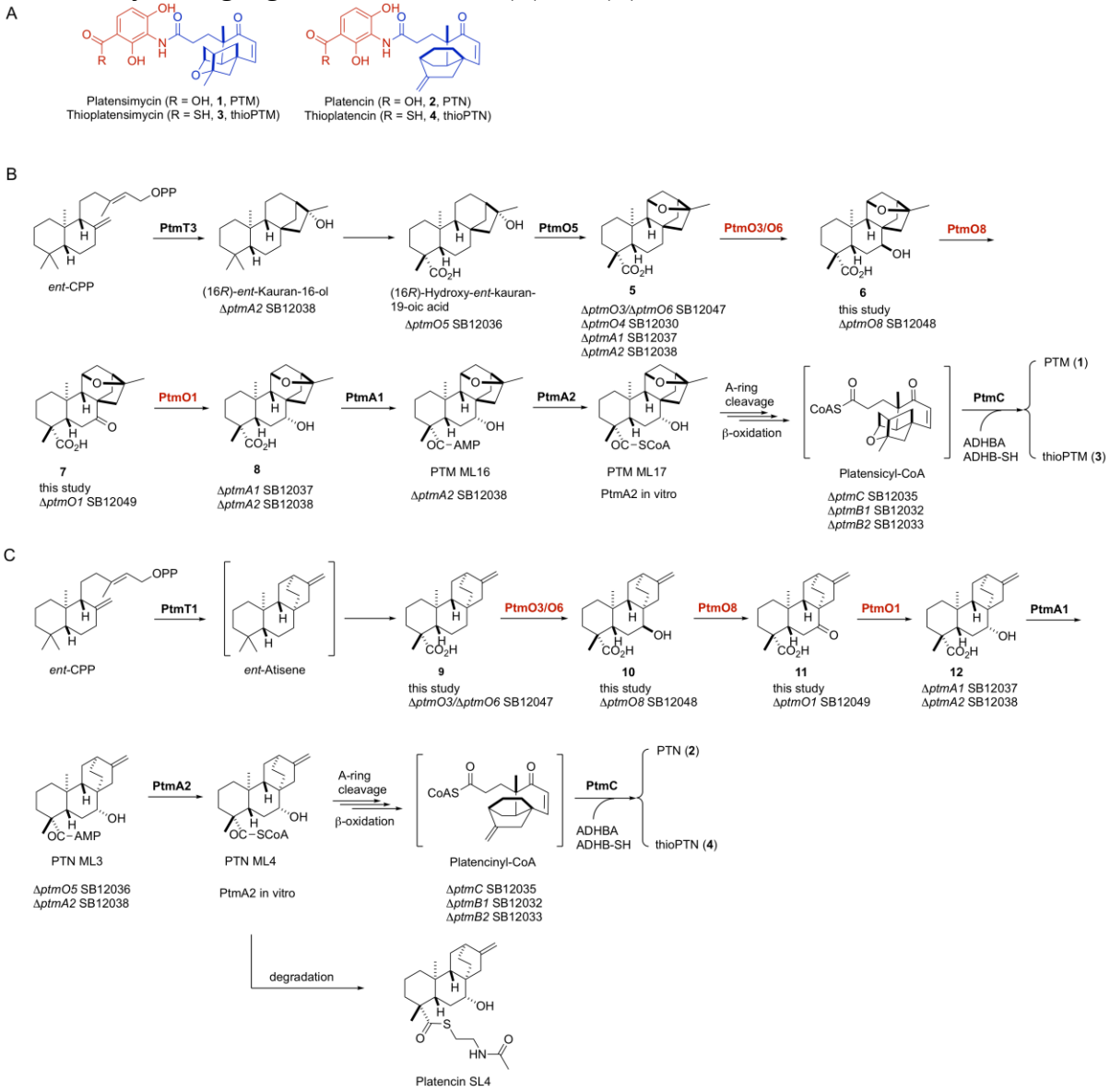

Figure S3. Southern analysis of the Δ*ptmR1*/Δ*ptmO3* double mutant *S. platensis* SB12045. (A) Schematic representation for the deletion of *ptmO3* in *S. platensis* SB12029 by insertion of an *aac(3)IV* + *oriT* cassette. The probe for *ptmO3* (509 bp) was amplified using the primers 739O3south_F and 739O3south_R and genomic DNAs as the template. (B) Southern blot verification of wild-type *ptmO3* (1631 bp) and double crossover Δ*ptmO3* (2184 bp) mutant genotypes. Lane 1, DNA marker VII, DIG-labeled (Roche); lane 2, *S. platensis* SB12029; lane 3, *S. platensis* SB12045.

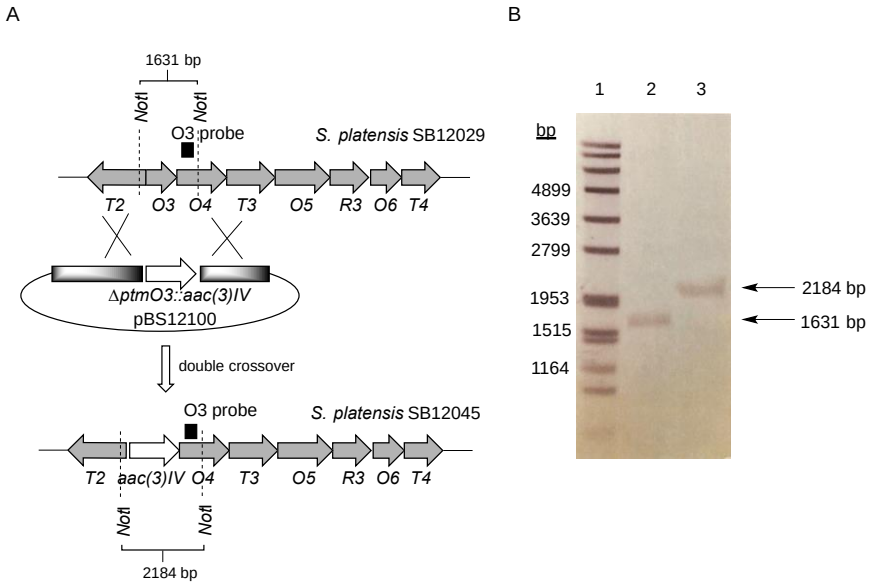

Figure S4. Southern analysis of the Δ*ptmR1*/Δ*ptmO6* double mutant *S. platensis* SB12046. (A) Schematic representation for the deletion of *ptmO6* in *S. platensis* SB12029 by insertion of an *aac(3)IV* + *oriT* cassette. The probe for *ptmO6* (621 bp) was amplified using the primers 739O6south_F and 739O6south_R and genomic DNAs as the template. (B) Southern blot verification of wild-type *ptmO6* (2732 bp) and double crossover Δ*ptmO6* (3285 bp) mutant genotypes. Lane 1, DNA marker VII, DIG-labeled (Roche); lane 2, *S. platensis* SB12029; lane 3, *S. platensis* SB12046.

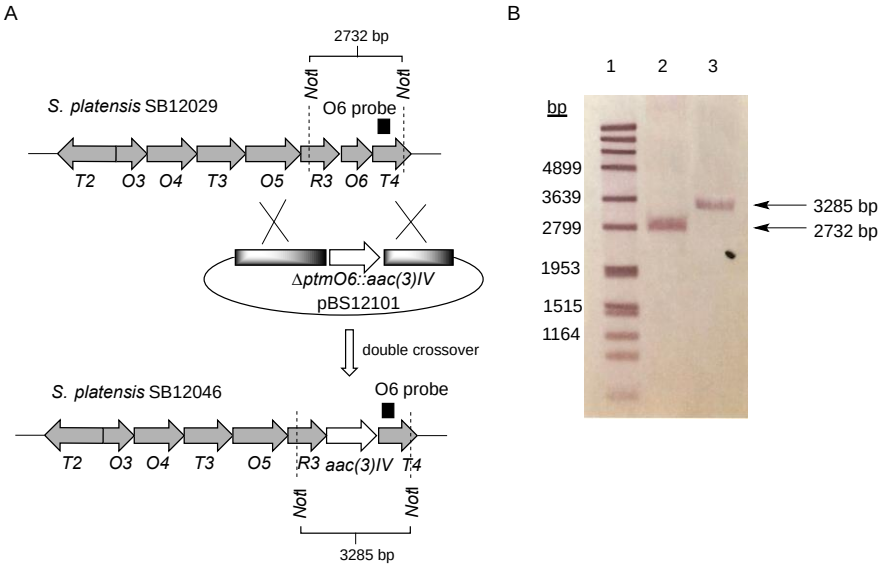

Figure S5. Southern analysis of the Δ*ptmR1*/Δ*ptmO3*/Δ*ptmO6* triple mutant *S. platensis* SB12047. (A) Schematic representation for the deletion of *ptmO3* as well as *ptmO6* (in-frame deletion) in *S. platensis* SB12029. The probe for *ptmO3* (509 bp) was amplified using the primers 739O3south_F and 739O3south_R and genomic DNAs as the template; The probe for *ptmO6* (621 bp) was amplified using the primers 739O6south_F and 739O6south_R and genomic DNAs as the template. (B) Southern blot verification of wild-type *ptmO3* (1631 bp) and double crossover Δ*ptmO3* (2184 bp) mutant genotypes as well as wild-type *ptmO6* (2732 bp) and in-frame double crossover Δ*ptmO6* (1997 bp) mutant genotypes. Lanes 1 and 4, DNA marker VII, DIG-labeled (Roche); lanes 2 and 5, *S. platensis* SB12029; lanes 3 and 6, *S. platensis* SB12047.

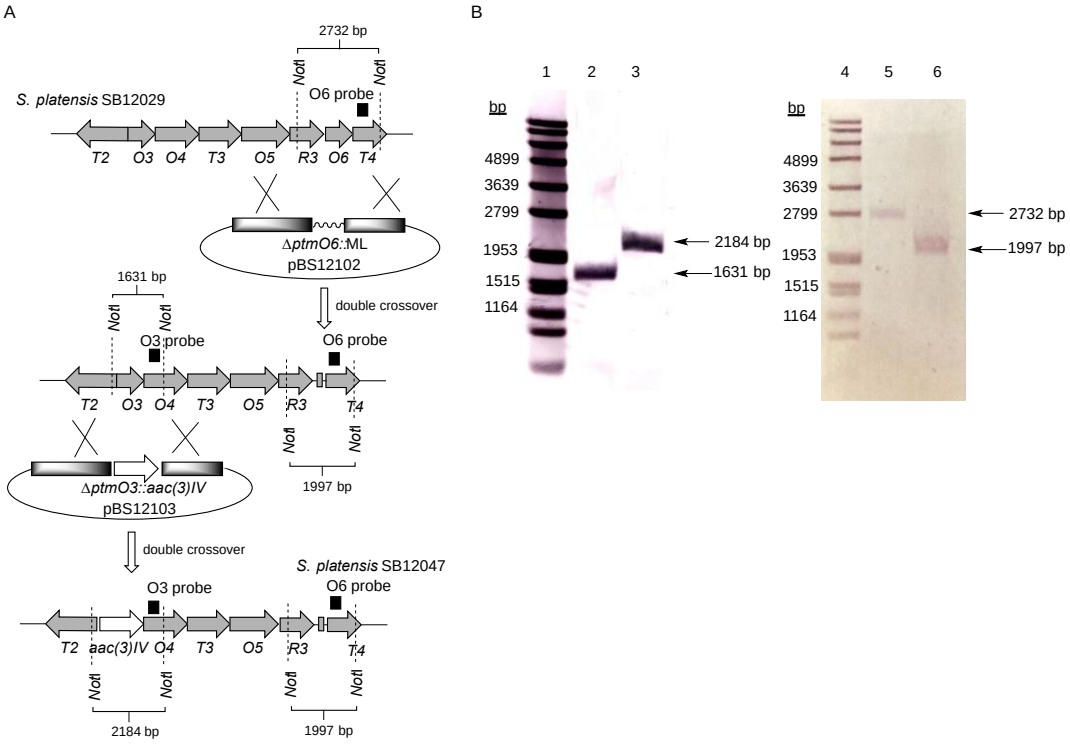

Figure S6. ^{1}H NMR spectrum of (11*S*,16*S*)-*ent*-kauran-11,16-epoxy-19-oic acid (**5**) in pyridine-d_5 (700 MHz).

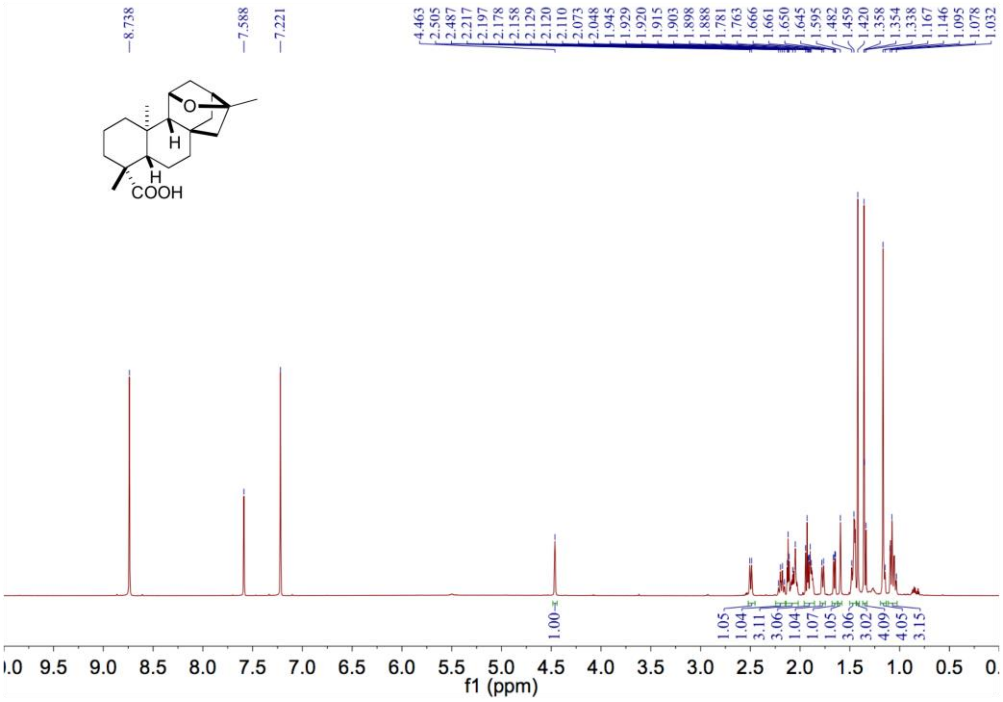

Figure S7. ^{13}C NMR spectrum of (11*S*,16*S*)-*ent*-kauran-11,16-epoxy-19-oic acid (**5**) in pyridine-d_5 (175 MHz).

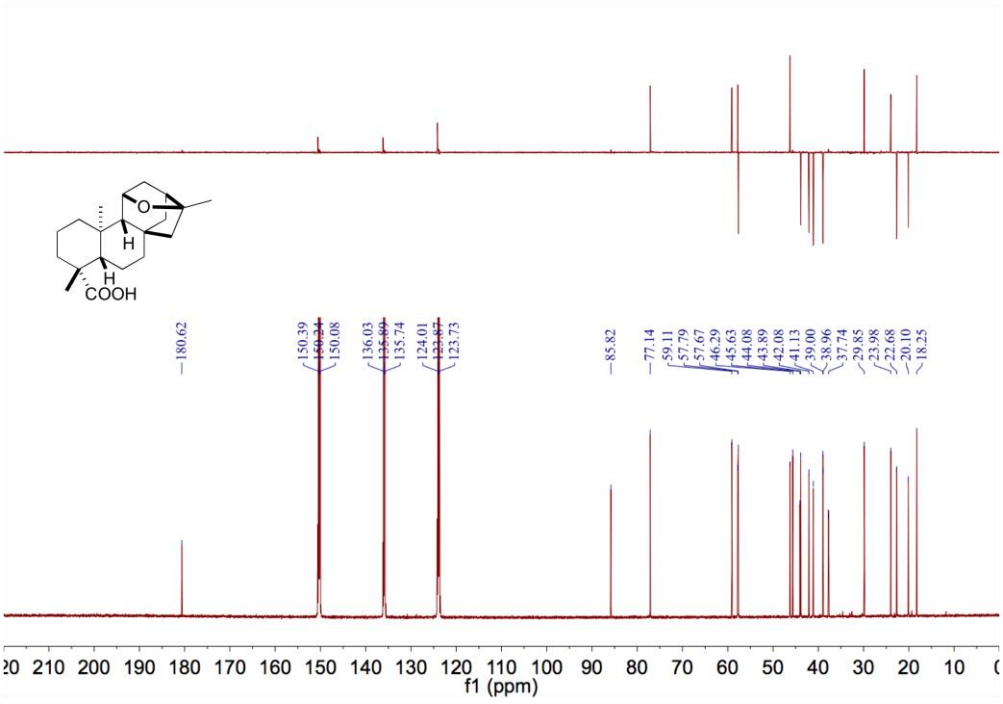

Figure S8. ^{1}H NMR spectrum of *ent*-atiser-16-en-19-oic acid (**9**) in $CDCl_3$ (700 MHz).

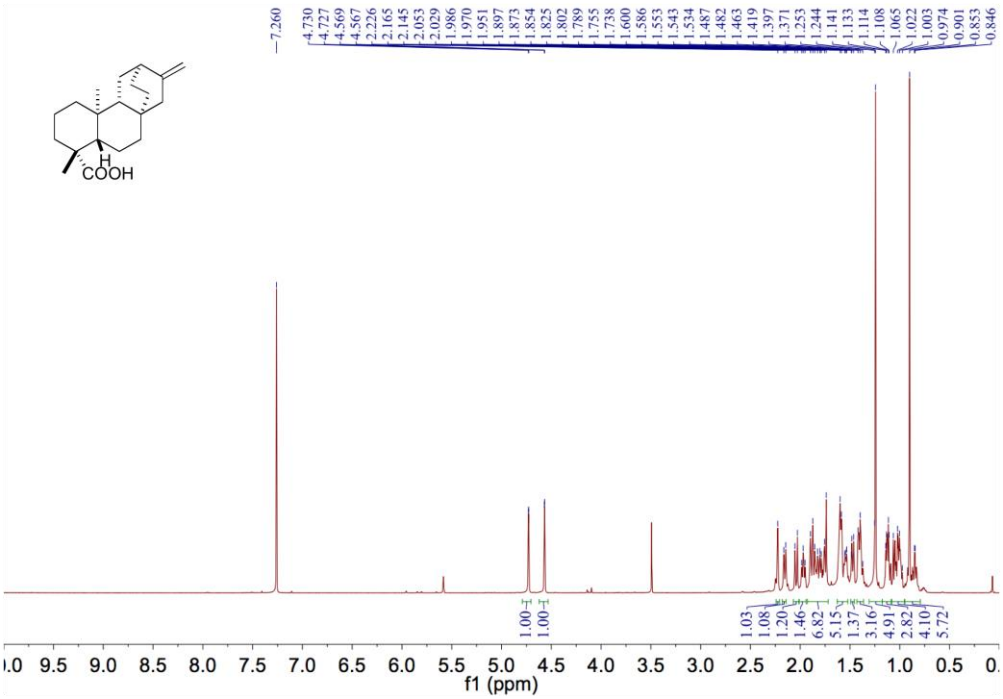

Figure S9. ^{13}C NMR spectrum of *ent*-atiser-16-en-19-oic acid (**9**) in $CDCl_3$ (175 MHz).

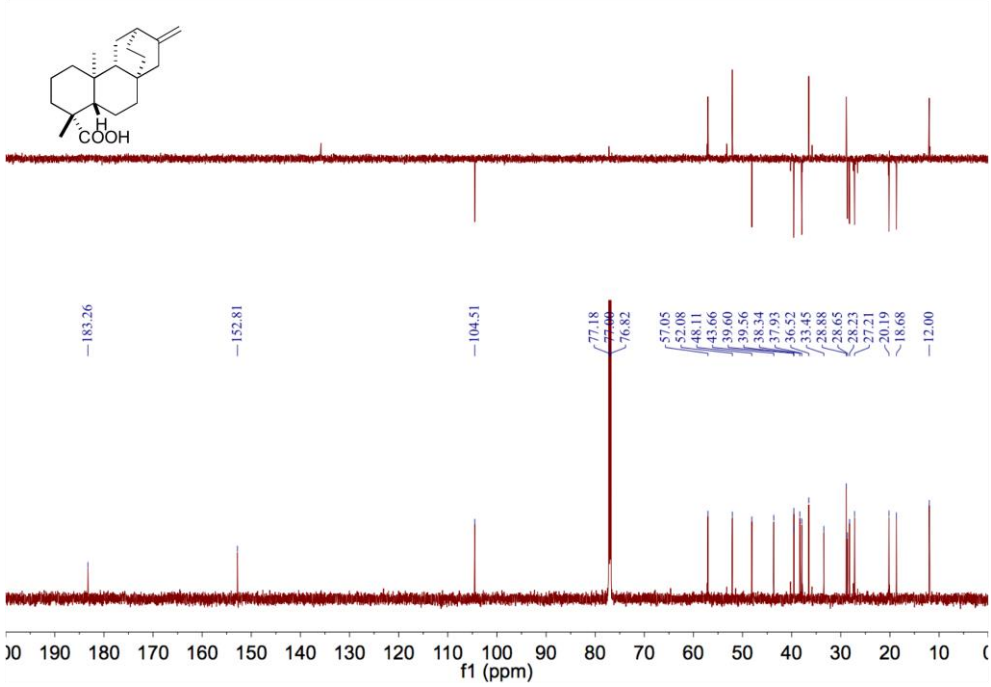

Figure S10. SDS-PAGE gel and size-exclusion chromatography of PtmO3 and PtmO6. (A) SDS-PAGE gel of purified PtmO3 and PtmO6. Lane 1, Unstained Protein Ladder (NEB); lane 2, purified N-His_6-PtmO3 (310 amino acids, ~33.7 kDa); lane 3, Color Prestained Protein Standard (NEB); lane 4, purified N-His_6-PtmO6 (305 amino acids, ~33.1 kDa). (B) Size-exclusion chromatography of PtmO3 and PtmO6. PtmO3 (red square) and PtmO6 (blue triangle) eluted at retention volumes of 77.2 and 78.1 mL, correlating to molecular weights (MWs) of 64.7 and 60.1 kDa, respectively. Thus, both PtmO3 and PtmO6 are supported as homodimers in solution.

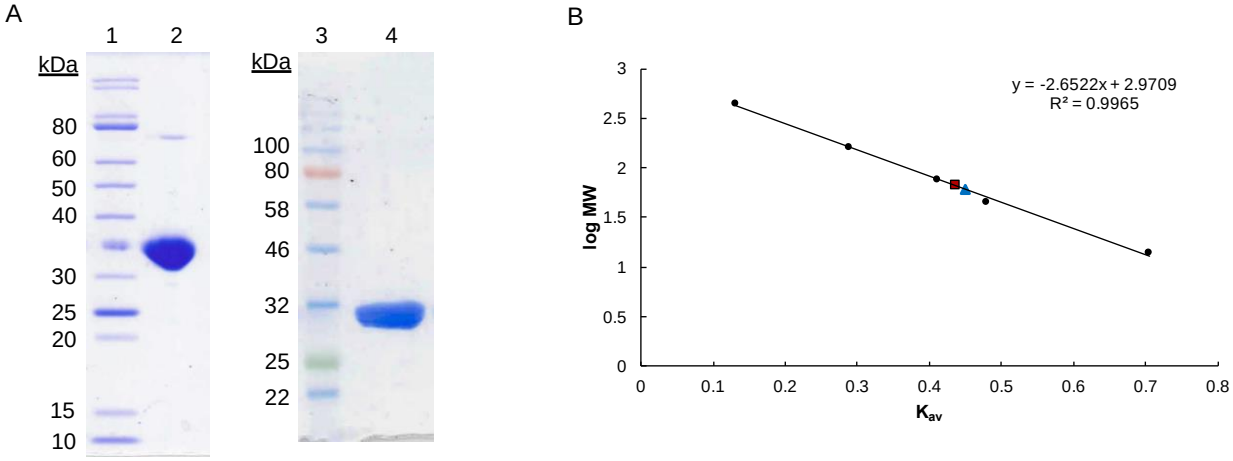

Figure S11. ^{1}H NMR spectrum of (7*S*)-hydroxy-(11*S*,16*S*)-11,16-epoxy-*ent*-kauran-19-oic acid (**6**) in DMSO-d_6 (700 MHz).

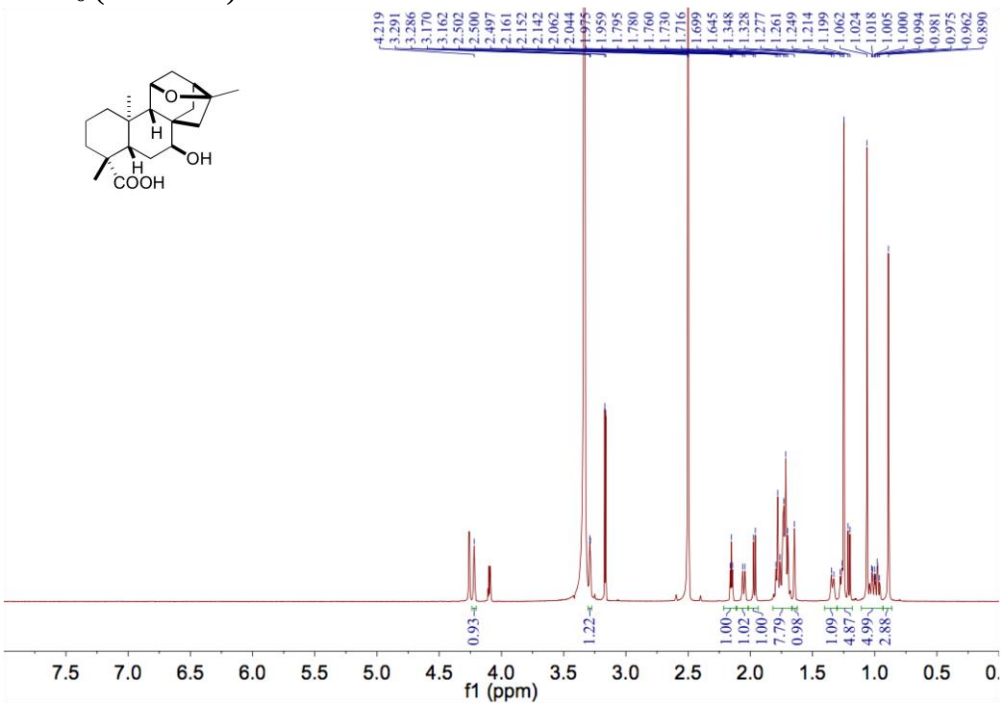

Figure S12. ^{13}C NMR spectrum of (7*S*)-hydroxy-(11*S*,16*S*)-11,16-epoxy-*ent*-kauran-19-oic acid (**6**) in DMSO-d_6 (175 MHz).

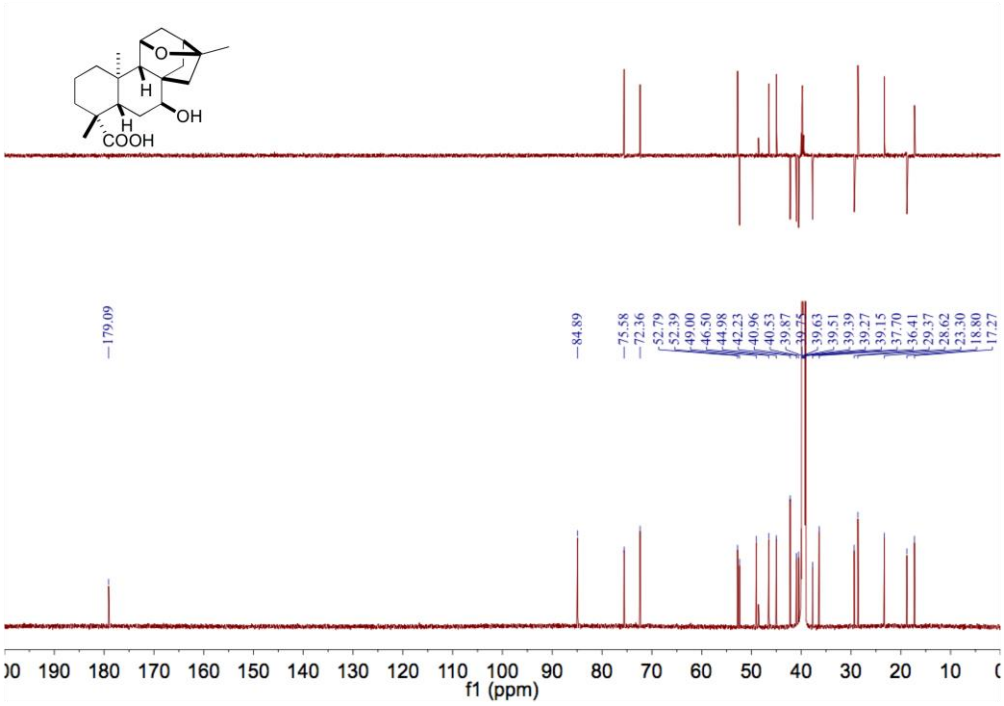

Figure S13. ^{1}H NMR spectrum of (7*S*)-hydroxy-(11*S*,16*S*)-11,16-epoxy-*ent*-kauran-19-oic acid (**6**) in pyridine-d_5 (700 MHz).

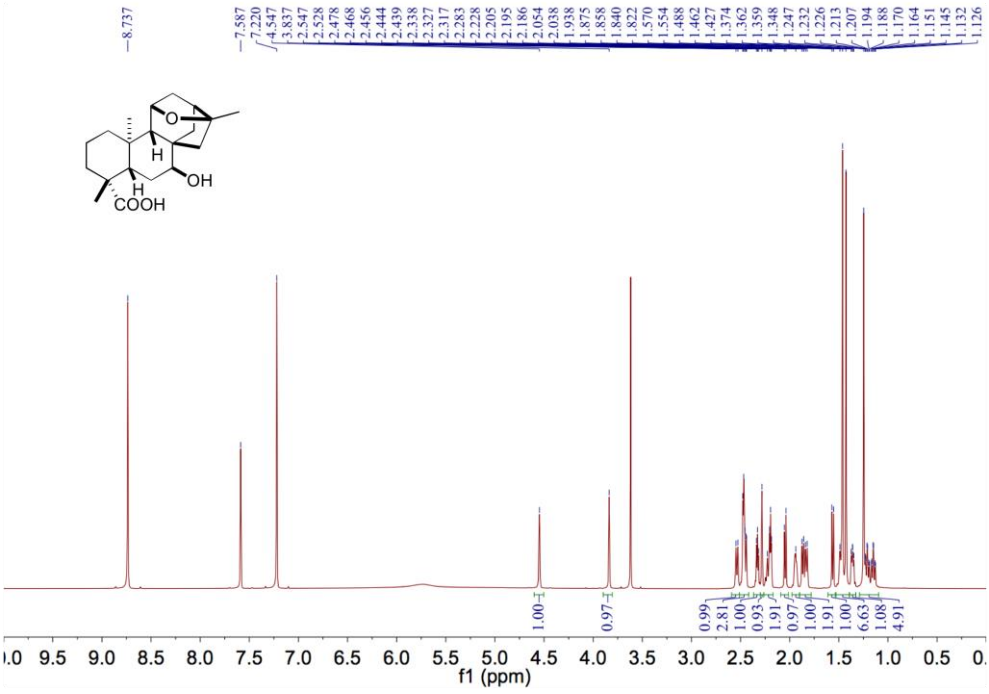

Figure S14. ^{13}C NMR spectrum of (7*S*)-hydroxy-(11*S*,16*S*)-11,16-epoxy-*ent*-kauran-19-oic acid (**6**) in pyridine-d_5 (175 MHz).

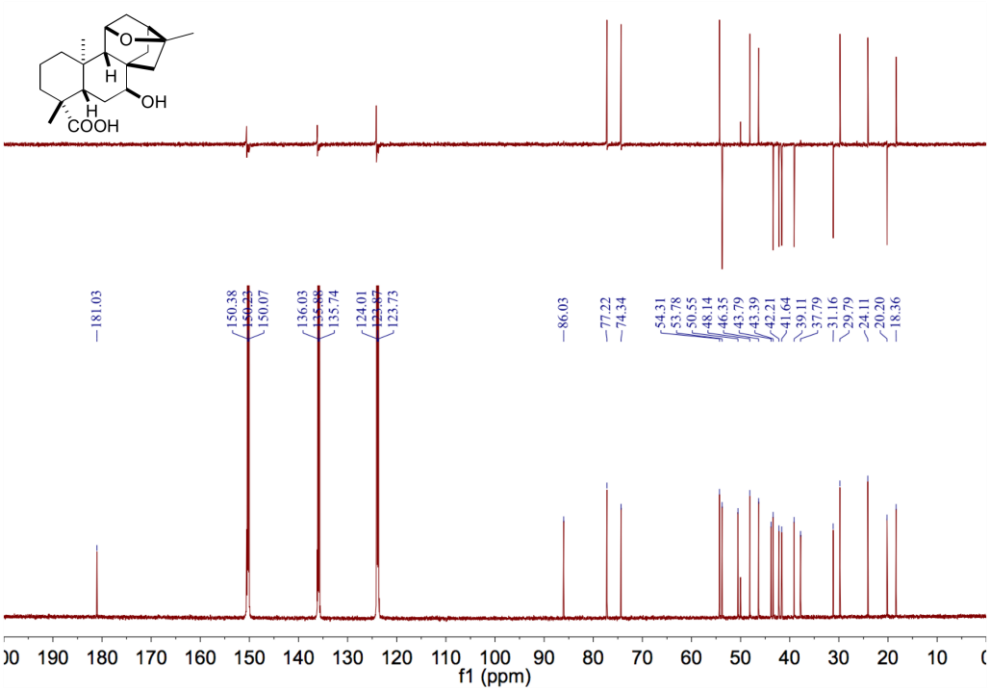

Figure S15. ^{1}H–^{1}H ROESY spectrum of (7*S*)-hydroxy-(11*S*,16*S*)-11,16-epoxy-*ent*-kauran-19-oic acid (**6**) in pyridine-d_5.

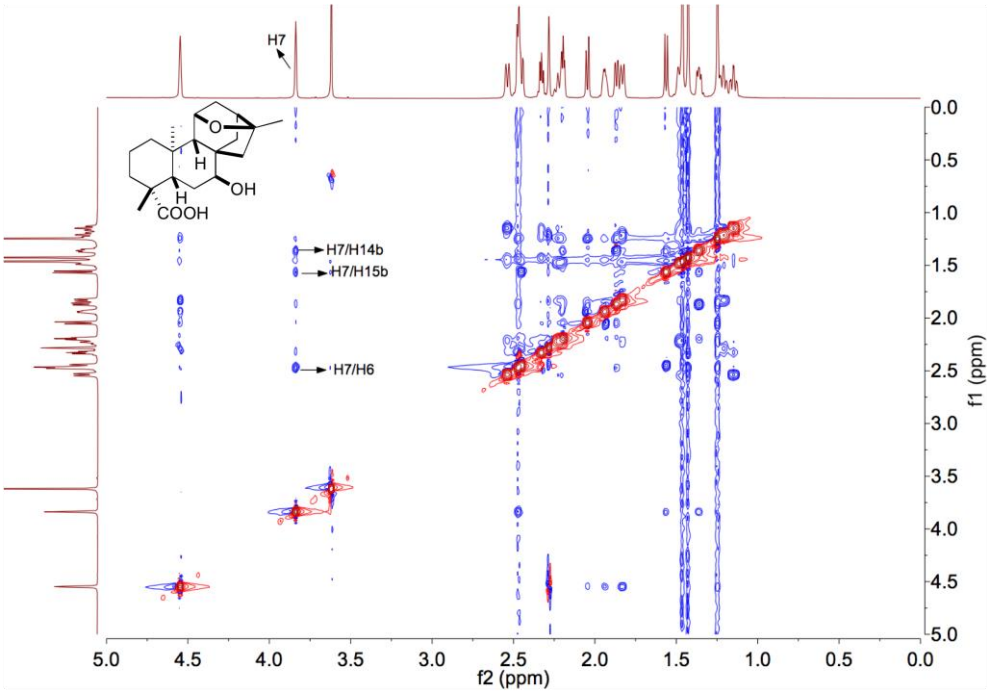

Figure S16. ^{1}H NMR spectrum of (7*S*)-7-hydroxy-*ent*-atiser-16-en-19-oic acid (**10**) in pyridine-d_5 (700 MHz).

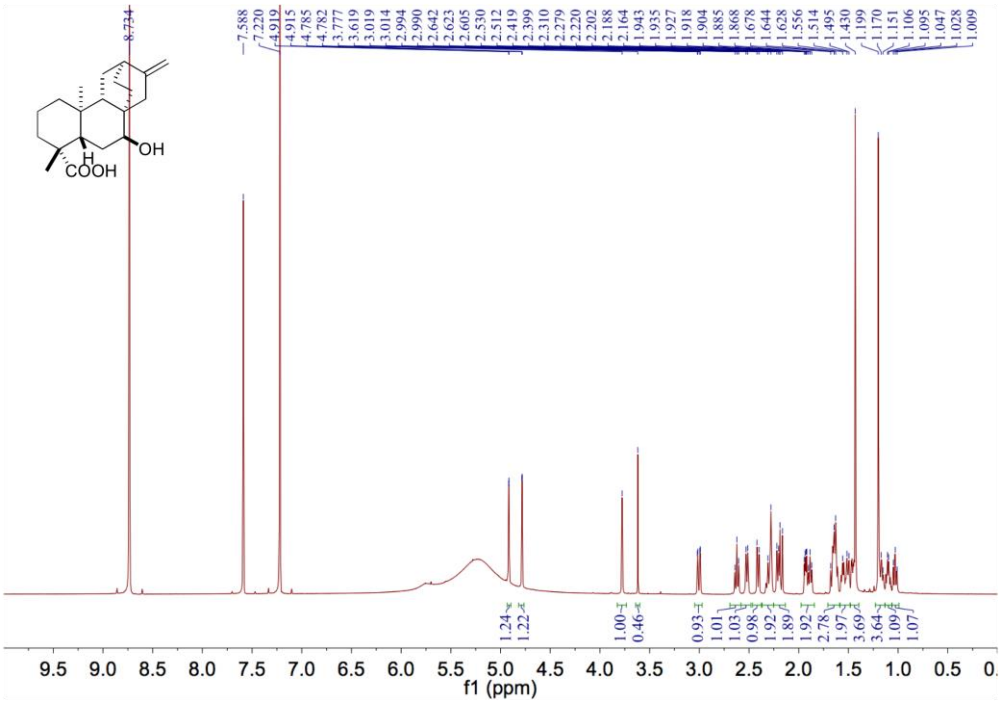

Figure S17. ^{13}C NMR spectrum of (7*S*)-7-hydroxy-*ent*-atiser-16-en-19-oic acid (**10**) in pyridine-d_5 (175 MHz).

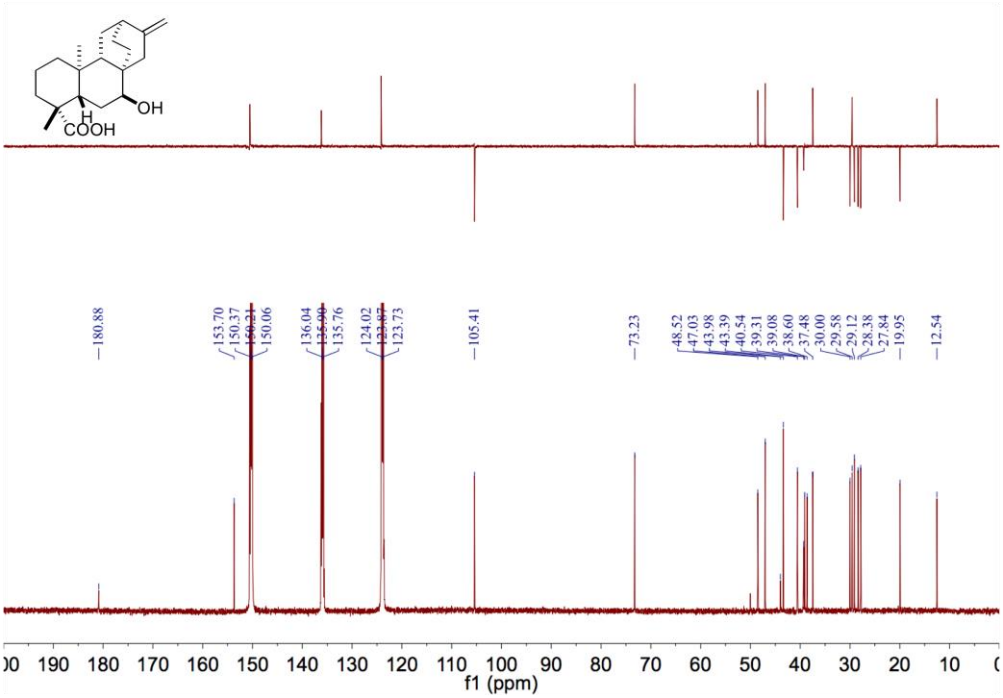

Figure S18. ^{1}H–^{1}H ROESY spectrum of (7*S*)-7-hydroxy-*ent*-atiser-16-en-19-oic acid (**10**) in pyridine-d_5.

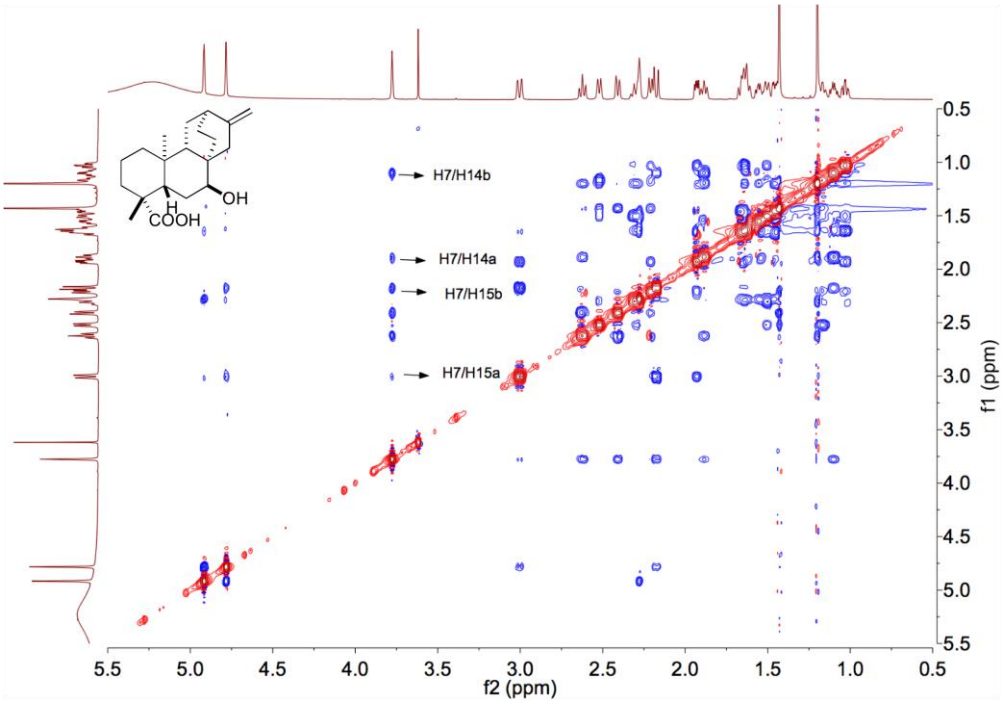

Figure S19. Steady-state kinetics of PtmO3 and PtmO6. Non-linear Michaelis-Menten regression plots of rate vs substrate concentrations were generated using GraphPad Prism 7 software (La Jolla, CA) to calculate the kinetic constants for each substrate. The determined kinetic parameters are summarized in Table 1 in the main text. Kinetics were performed in triplicate and each data point represents the mean of the three independent assays with error bars representing the standard deviation. (A) PtmO3 (20 nM) was incubated with varying concentrations (2–150 μM) of **5**. (B) PtmO3 (20 nM) was incubated with varying concentrations (2–150 μM) of **9**. (C) PtmO6 (20 nM) was incubated with varying concentrations (2–150 μM) of **5**. (D) PtmO6 (20 nM) was incubated with varying concentrations (1–50 μM) of **9**.

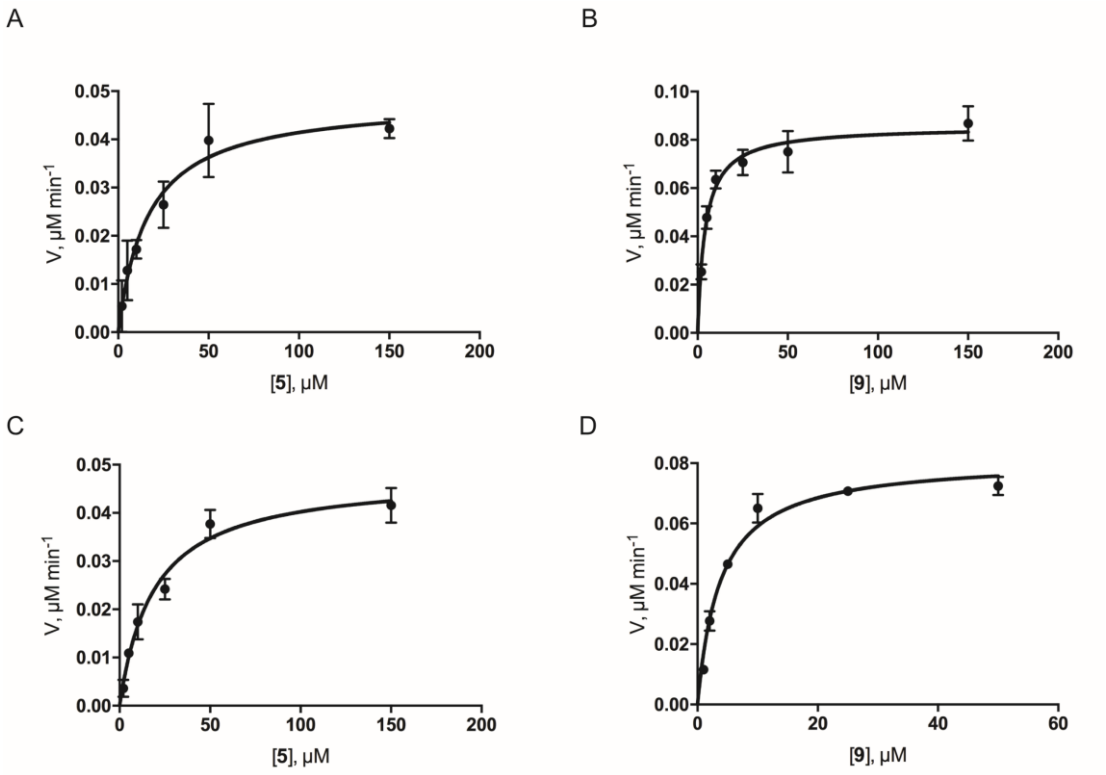

Figure S20. ^{1}H NMR spectrum of (11*S*,16*S*)-methyl-*ent*-kauran-11,16-epoxy-19-oate (**13**) in $CDCl_3$ (600 MHz).

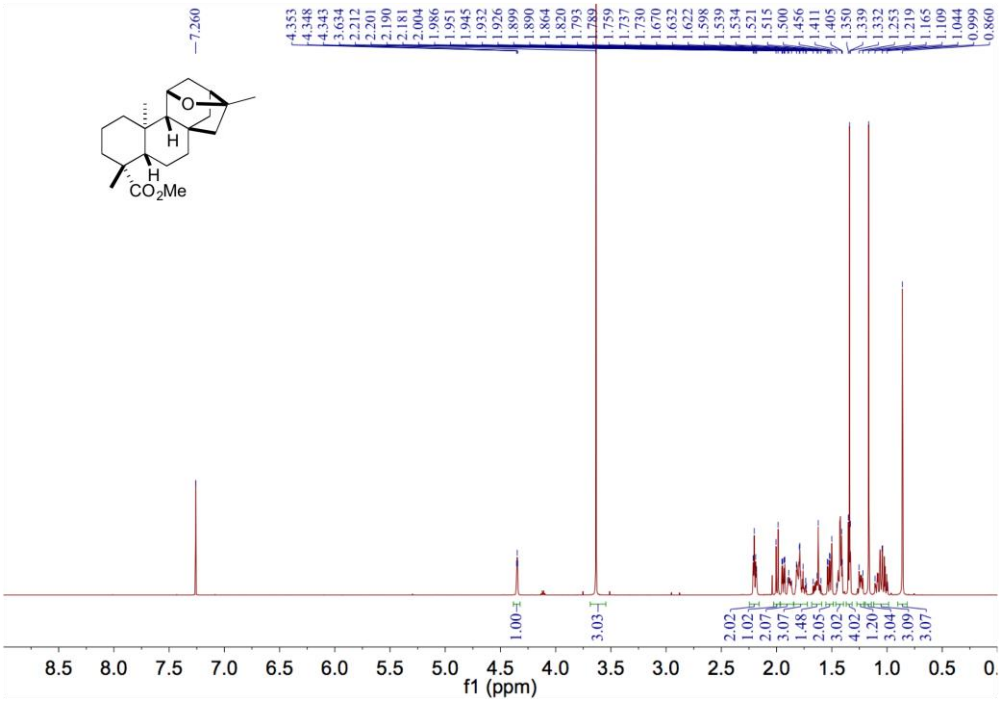

Figure S21. ^{13}C NMR spectrum of (11*S*,16*S*)-methyl-*ent*-kauran-11,16-epoxy-19-oate (**13**) in $CDCl_3$ (150 MHz).

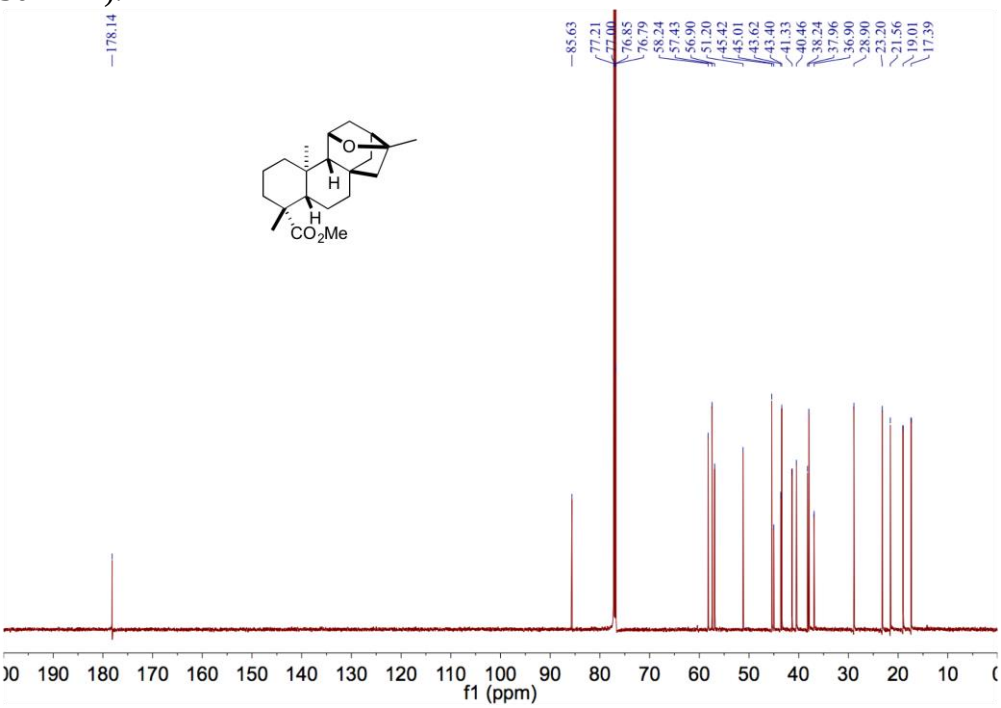

Figure S22. ^{1}H NMR spectrum of C19-iodo derivative **5-I** in $CDCl_3$ (600 MHz).

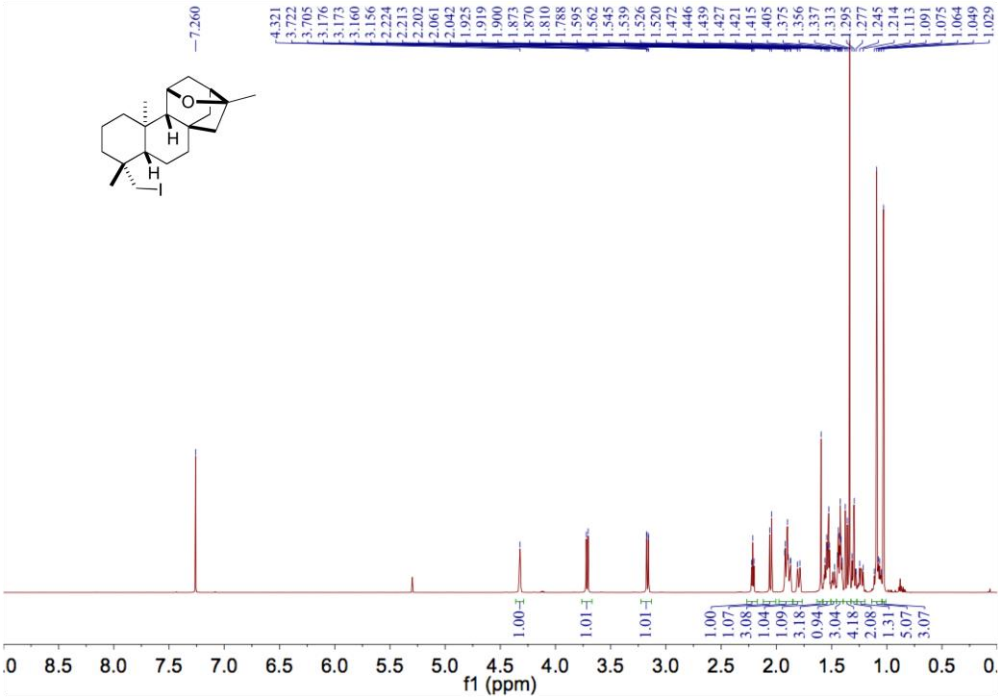

Figure S23. ^{13}C NMR spectrum C19-iodo derivative of **5-I** in $CDCl_3$ (150 MHz).

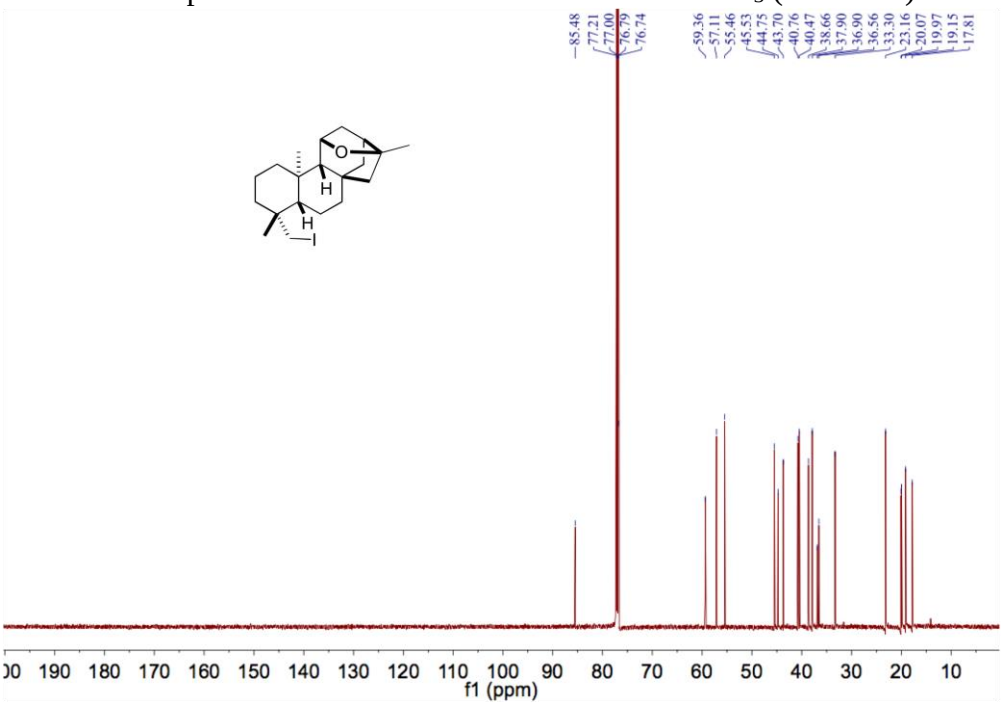

Figure S24. ^{1}H NMR spectrum of C4 *gem*-dimethyl derivative **14** in $CDCl_3$ (600 MHz).

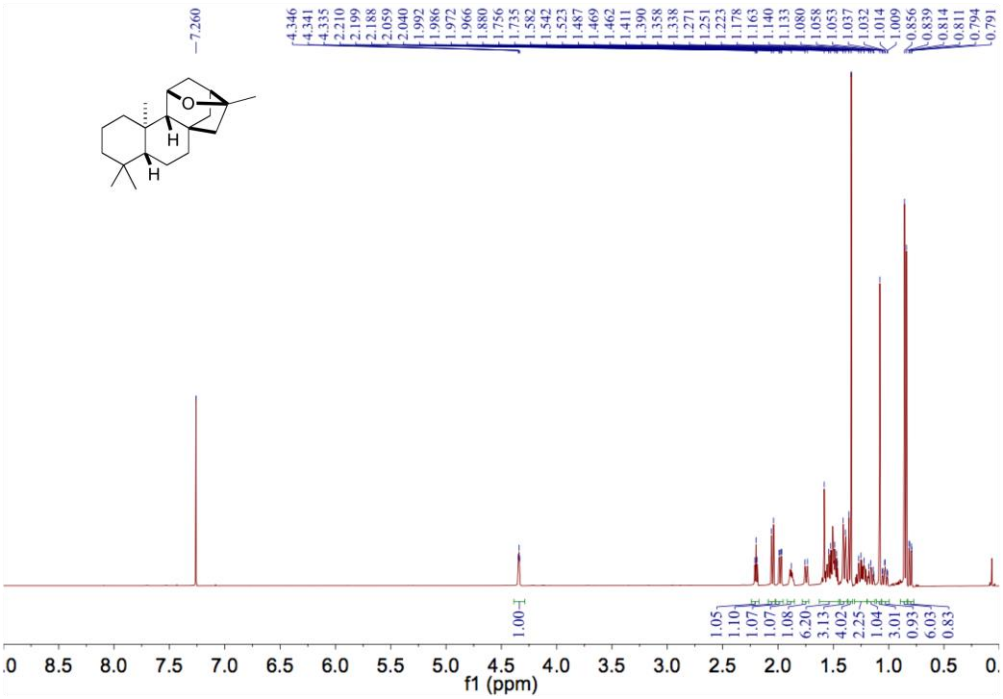

Figure S25. ^{13}C NMR spectrum of C4 *gem*-dimethyl derivative **14** in $CDCl_3$ (150 MHz).

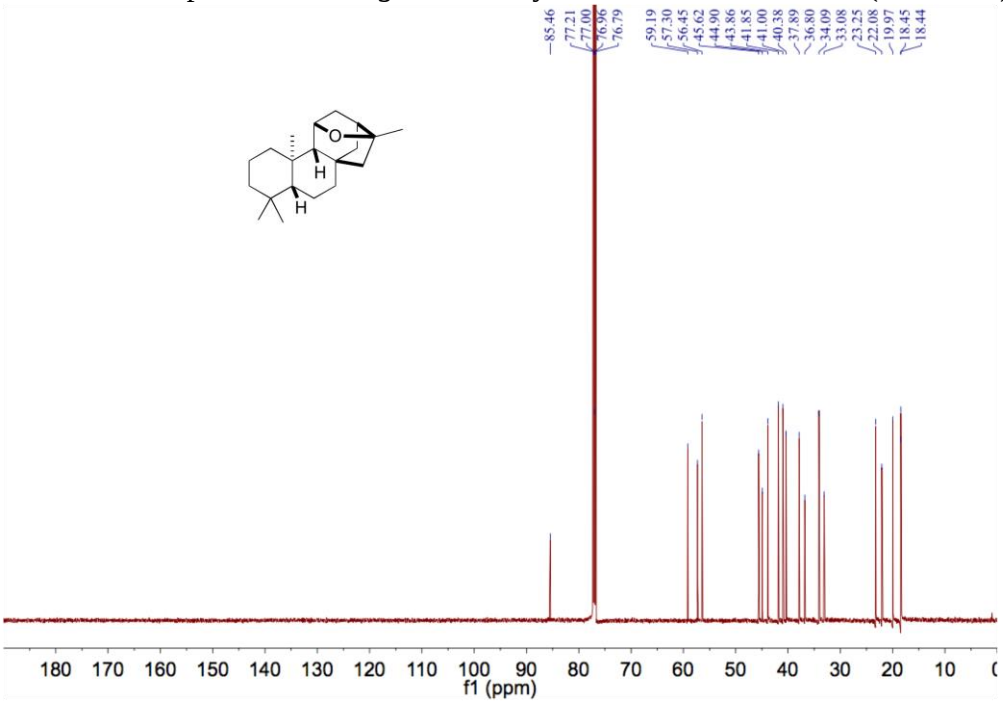

Figure S26. Homology modeling and docking of substrates in PtmO6. (A) View of the overall structure of PtmO6. The modeling was generated using the I-TASSER online server and shows a high C-score of 1.3.[15] (B) Conserved residues responsible for binding of α-ketoglutarate (α-KG) and Fe^{II} are shown. The PtmO6 homology model was docked with **5** (green, C) and **9** (cyan, D) with the residues proposed for positioning the diterpenoid substrates with the β hydrogen of C7 (magenta) oriented towards Fe^{II}. (E) Sequence alignment of selected Fe/α-KG dioxygenases from bacteria. Aligned residues are colored based on the level of conservation (red box with white character shows strict identity, red character similarity, and blue frame similarity across groups). The conserved triad (His93, Asp95, and His240 in 739O6) binding to Fe and residues (Thr120, Arg251, and Arg255 in 739O6) binding to α-KG are shown with blue and pink asterisks, respectively. The conserved residues highlighted in (E) of PtmO6 are shown in (B). The protein sequences were obtained from the NCBI database: 739O3 (*S. platensis* CB00739; AIW55556), 739O6 (*S. platensis* CB00739; AIW55561), 7327O3 (*S. platensis* MA7327; ACO31277), 7327O6 (*S. platensis* MA7327; ACO31282), 7339O6 (*S. platensis* MA7339; ADD83004), TauD (*E. coli*; PDB ID: 1GQW), CAS1 (*S. clavuligerus*; PDB ID: 1DS1), AtsK (*Pseudomonas putida*; PDB ID: 1VZ4), and PvcB (*Pseudomonas aeruginosa*; PDB ID: 3EAT). The alignment was created with MUSCLE[26] and rendered with ESPript 3.0[27].

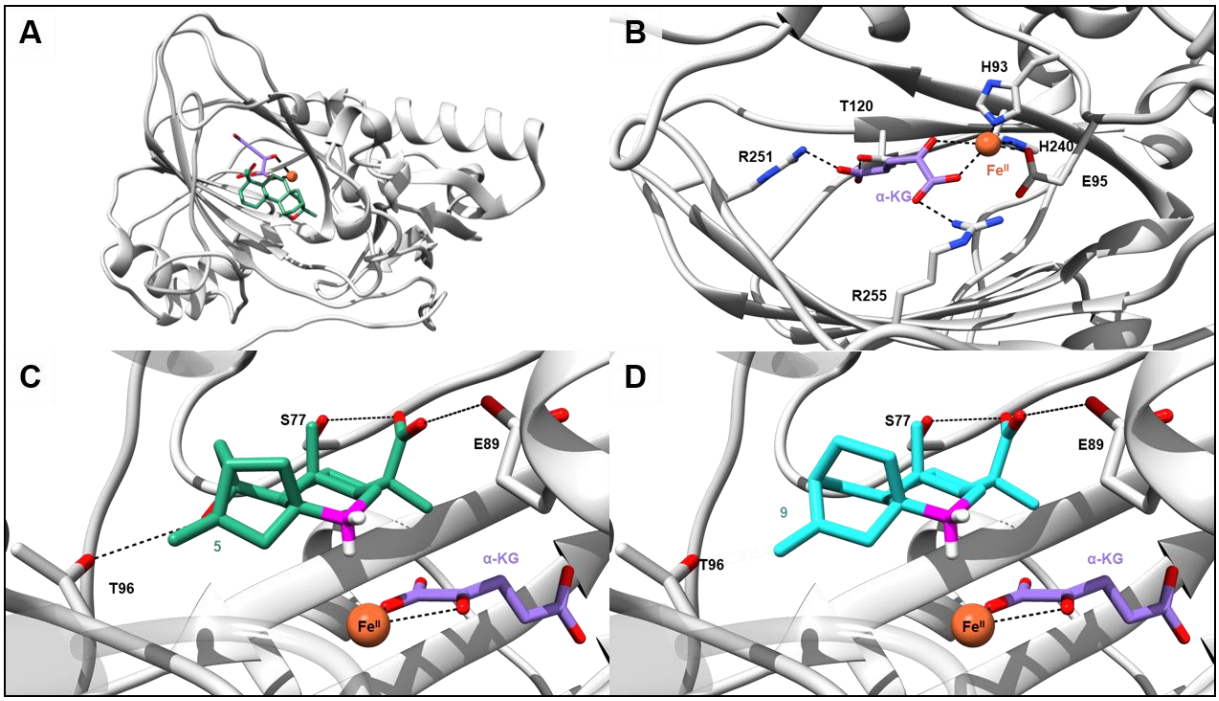

Figure S26 cont. (E) Sequence alignment of selected α-ketoglutarate-dependent dioxygenases from bacteria.

E

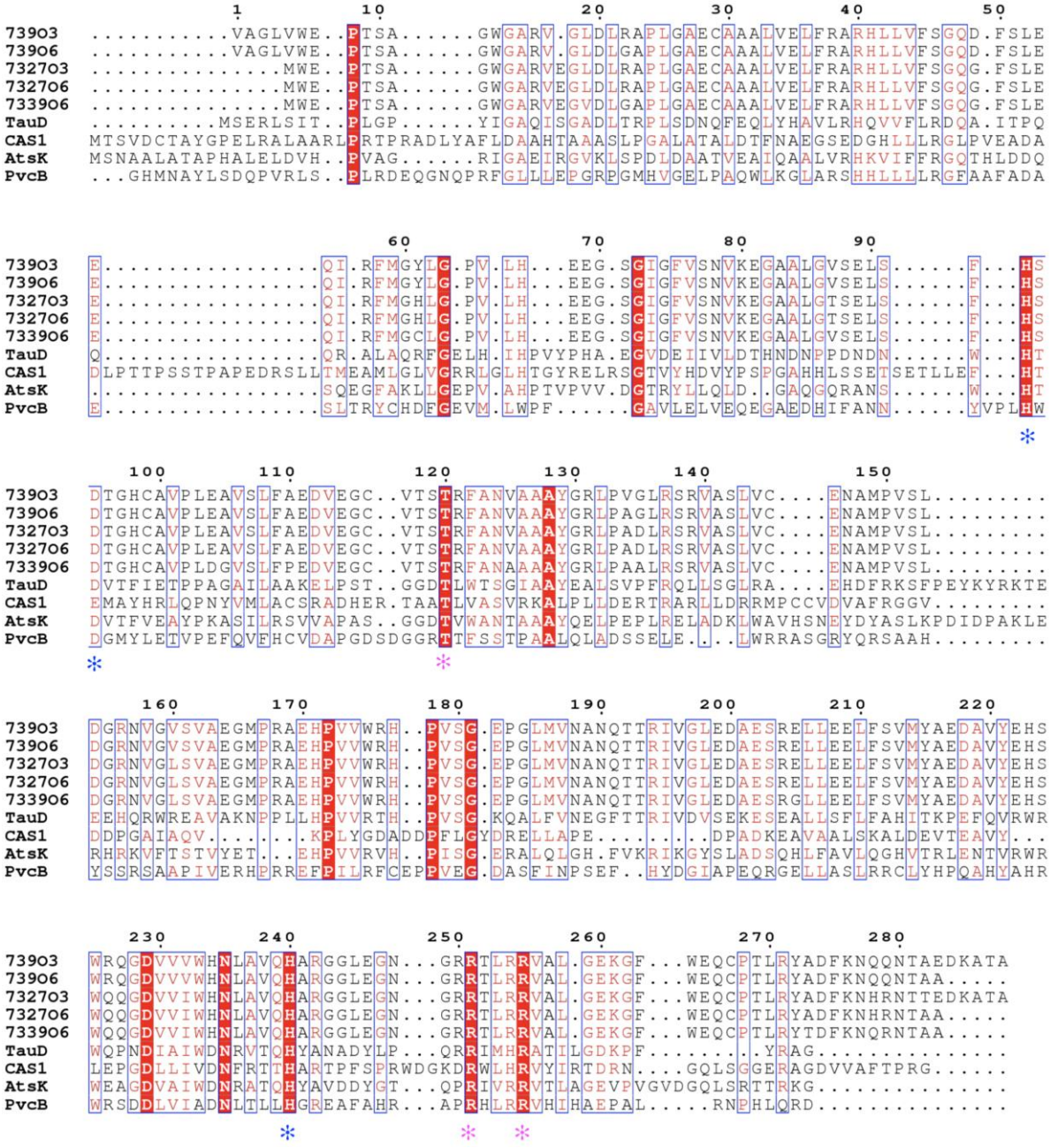

Figure S27. A proposed mechanism of stereoselective hydroxylation of PtmO6 with substrates **5** (A) and **9** (B). The H_β of C7 positions closely to the high-valent Fe^{IV} intermediate, which is able to abstract this hydrogen and generate a radical (**5-radical** or **9-radical**) that rebounds to the incipient Fe^{III}-OH to form the C7 β hydroxyls observed in **6** and **10**. (C) ORTEP drawing of crystal structure of **5** (CCDC 1894472). (D) 3D model of **5-radical** generated by ChemDraw 3D (MM2 energy-minimized) showing a minor conformational change of the B-ring.

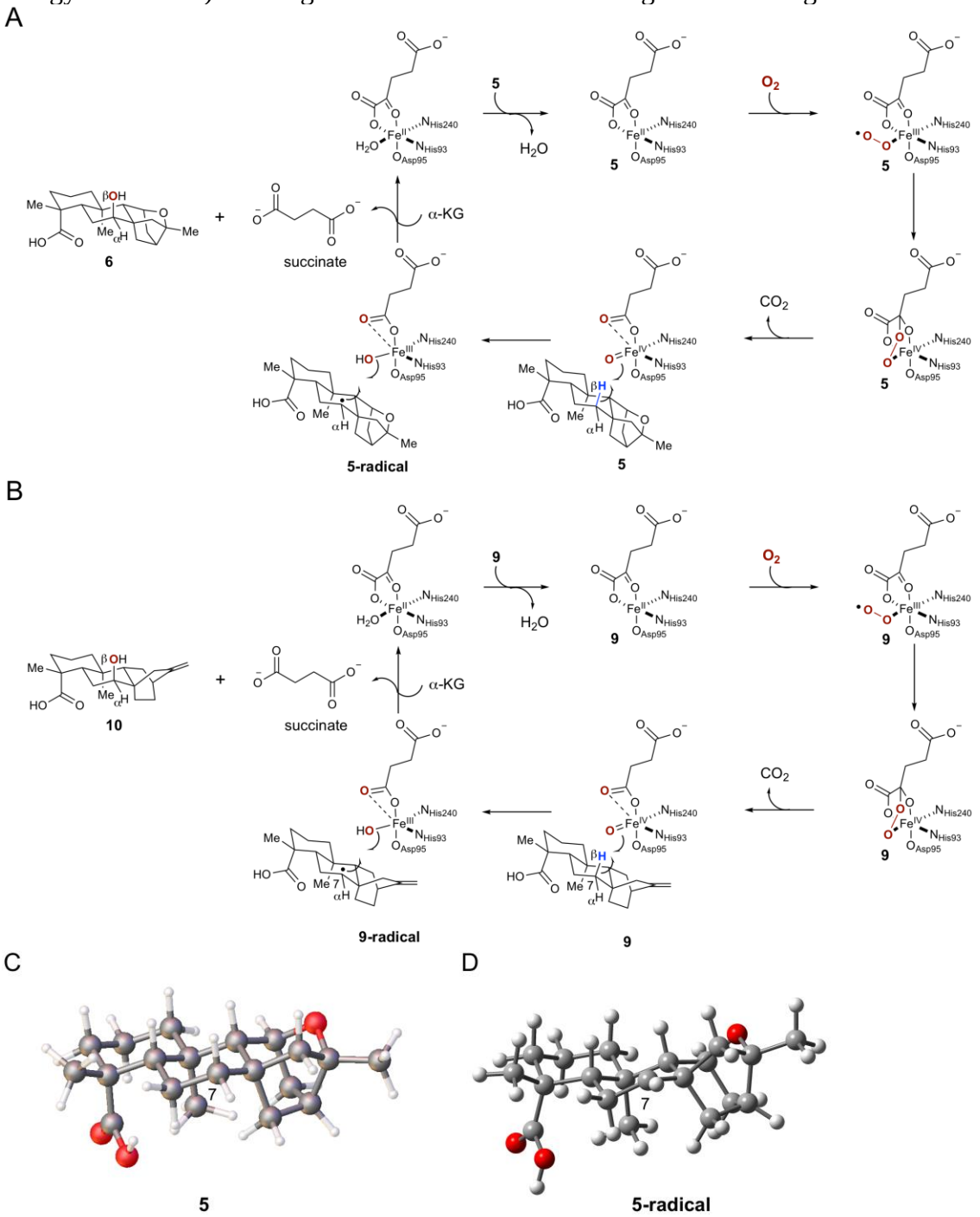

Figure S28. Southern analysis of the Δ*ptmR1*/Δ*ptmO8* double mutant *S. platensis* SB12048. (A) Schematic representation for the deletion of *ptmR1* and *ptmO8* in *S. platensis* CB00739 by insertion of an *aac(3)IV* + *oriT* cassette. The probe for *ptmR1* and *ptmO8* (549 bp) was amplified using the primers 739R1O8south_F and 739R1O8south_R and genomic DNAs as the template. (B) Southern blot verification of wild-type *ptmR1* and *ptmO8* (3287 bp) and double crossover Δ*ptmR1*/Δ*ptmO8* (2870 bp) mutant genotypes. Lane 1, DNA marker VII, DIG-labeled (Roche); lane 2, *S. platensis* CB00739; lane 3, *S. platensis* SB12048.

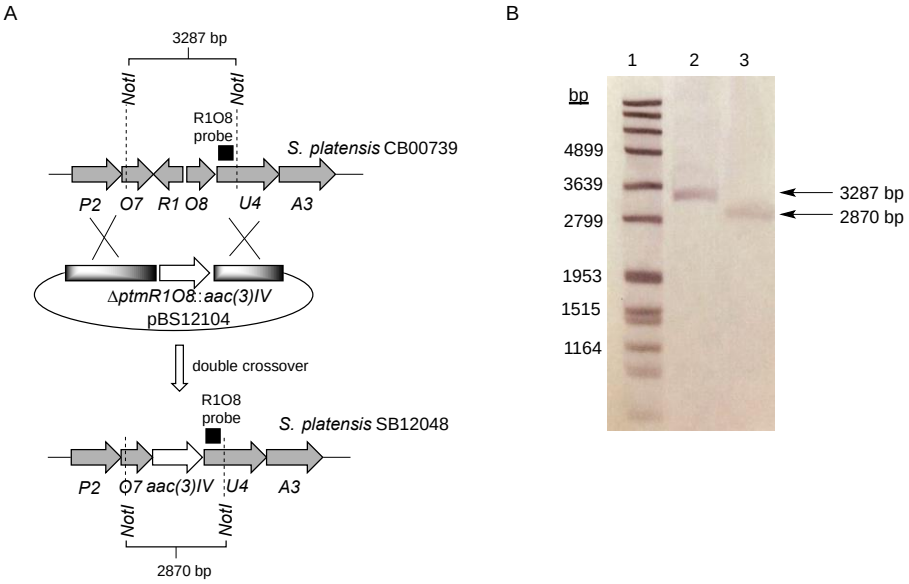

Figure S29. Southern analysis of the Δ*ptmR1*/Δ*ptmO1* double mutant *S. platensis* SB12049. (A) Schematic representation for the deletion of *ptmO1* in *S. platensis* SB12029 by insertion of an *aac(3)IV* + *oriT* cassette. The probe for *ptmO1* (603 bp) was amplified using the primers 739O1south_F and 739O1south_R and genomic DNAs as the template. (B) Southern blot verification of wild-type *ptmO1* (1490 bp) and double crossover Δ*ptmO1* (2322 bp) mutant genotypes. Lane 1, DNA marker VII, DIG-labeled (Roche); lane 2, *S. platensis* SB12029; lane 3, *S. platensis* SB12049.

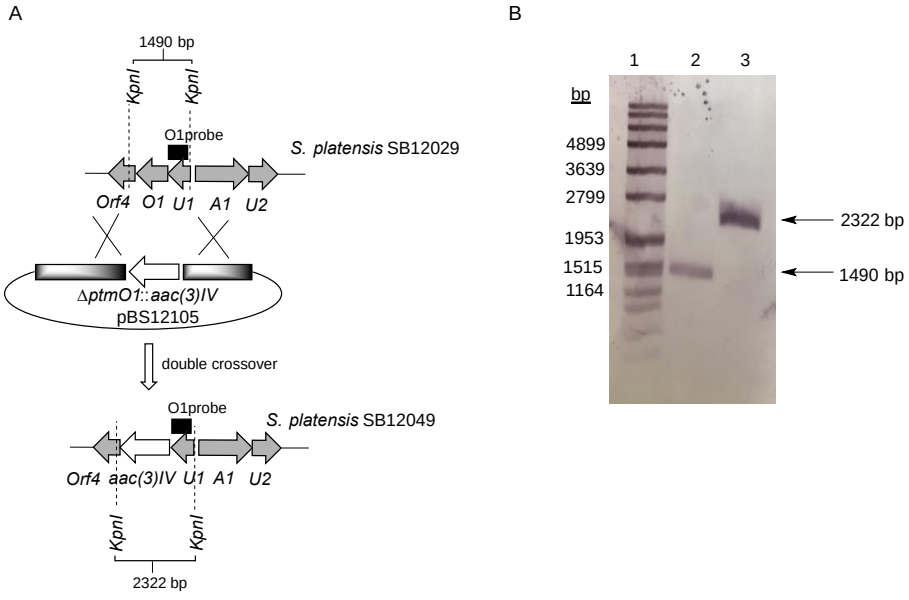

Figure S30. ^{1}H NMR spectrum of 7-oxo-(11*S*,16*S*)-11,16-epoxy-*ent*-kauran-19-oic acid (**7**) in pyridine-d_5 (700 MHz).

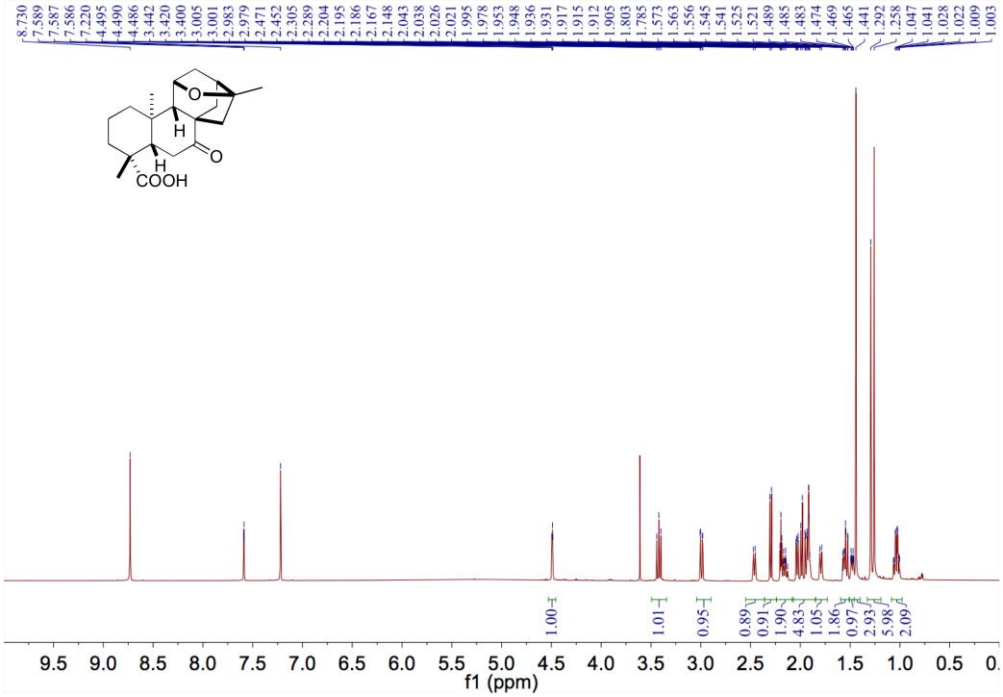

Figure S31. ^{13}C NMR spectrum of 7-oxo-(11*S*,16*S*)-11,16-epoxy-*ent*-kauran-19-oic acid (**7**) in pyridine-d_5 (175 MHz).

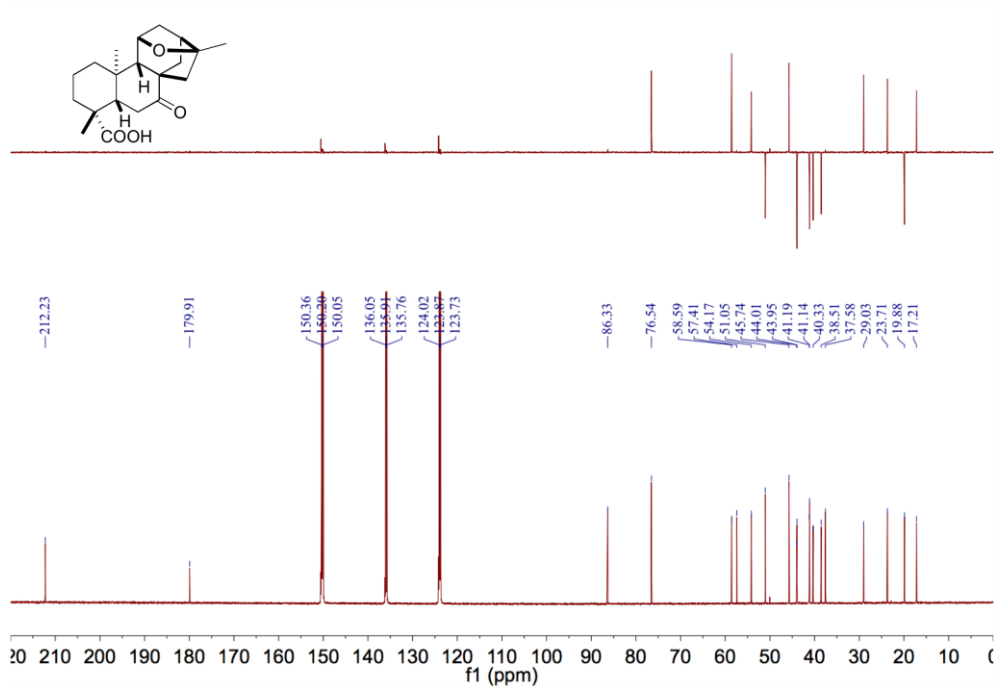

Figure S32. ^{1}H NMR spectrum of 7-oxo-*ent*-atiser-16-en-19-oic acid (**11**) in $CDCl_3$ (700 MHz)

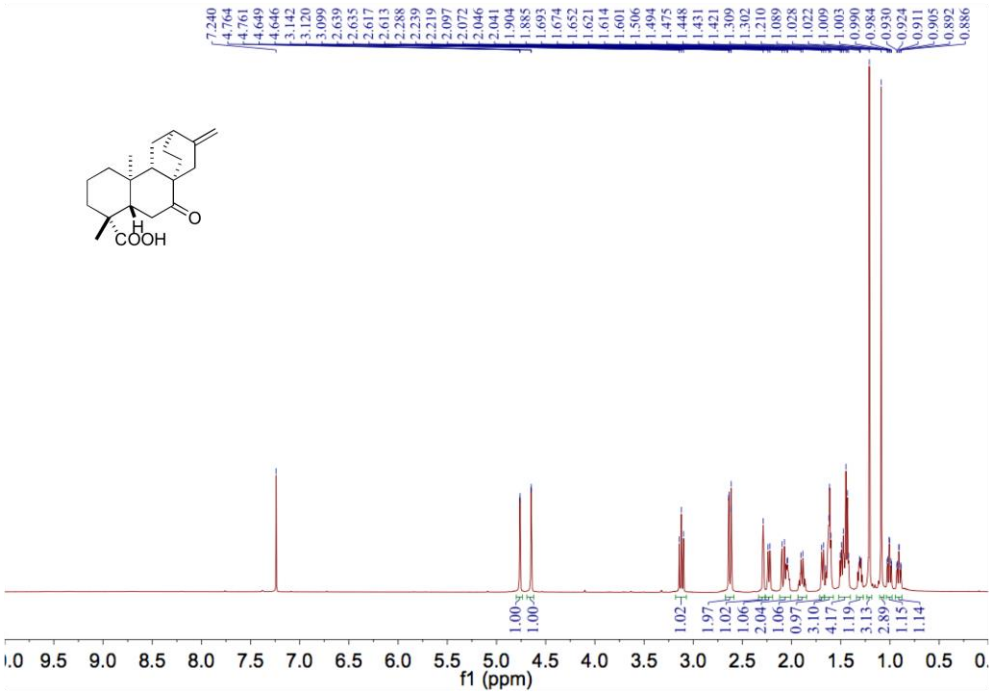

Figure S33. ^{13}C NMR spectrum of 7-oxo-*ent*-atiser-16-en-19-oic acid (**11**) in $CDCl_3$ (175 MHz)

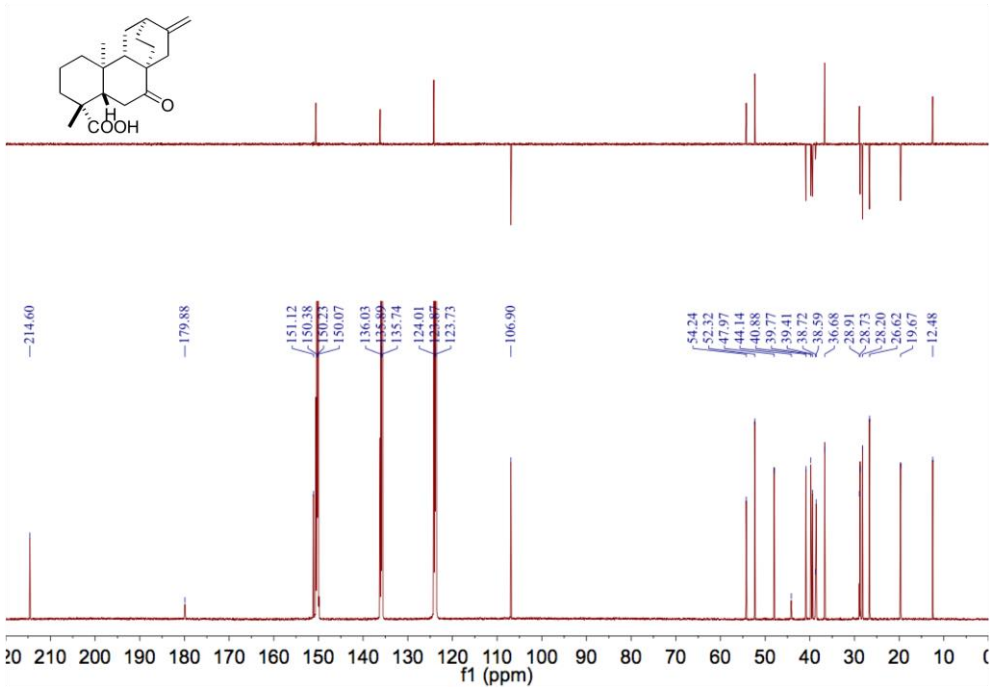

Figure S34. ^{1}H NMR spectrum of 7-oxo-*ent*-atiser-16-en-19-oic acid (**11**) in pyridine-d_5 (700 MHz)

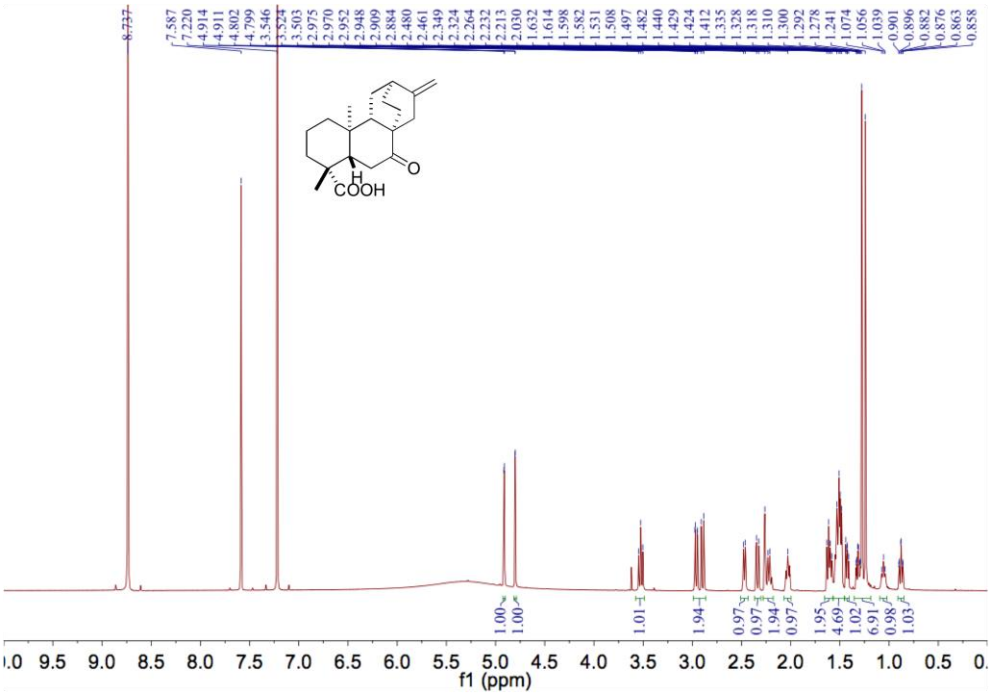

Figure S35. ^{13}C NMR spectrum of 7-oxo-*ent*-atiser-16-en-19-oic acid (**11**) in pyridine-d_5 (175 MHz)

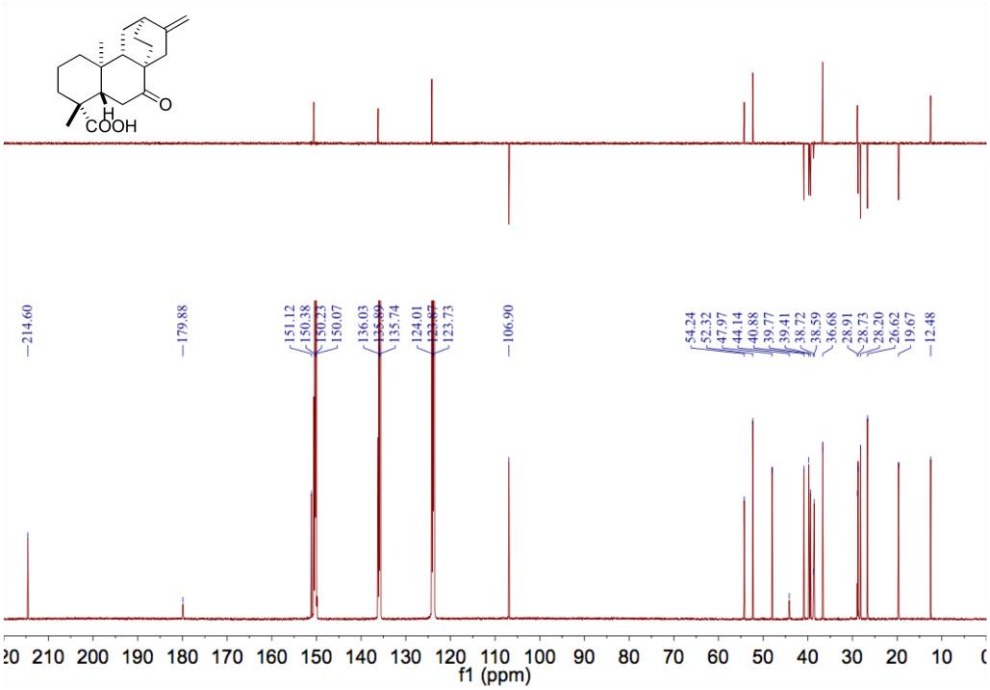

Figure S36. SDS-PAGE gel and size-exclusion chromatography of PtmO8 and PtmO1. (A) SDS-PAGE gel of purified PtmO8 and PtmO1. Lanes 1 and 5, Color Prestained Protein Standard (NEB); lanes 2–4, purified N-His_6-PtmO8 (285 amino acids, ~29.4 kDa); lane 6, purified N-His_6-PtmO1 (276 amino acids, ~29.2 kDa). (B) Size-exclusion chromatography of PtmO8 and PtmO1. PtmO8 (blue triangle) and PtmO1 (red square) eluted at retention volumes of 68.6 and 69.6 mL, correlating to molecular weights (MWs) of 129.3 and 119.7 kDa, respectively. Thus, both PtmO8 and PtmO1 are supported as homotetramers in solution.

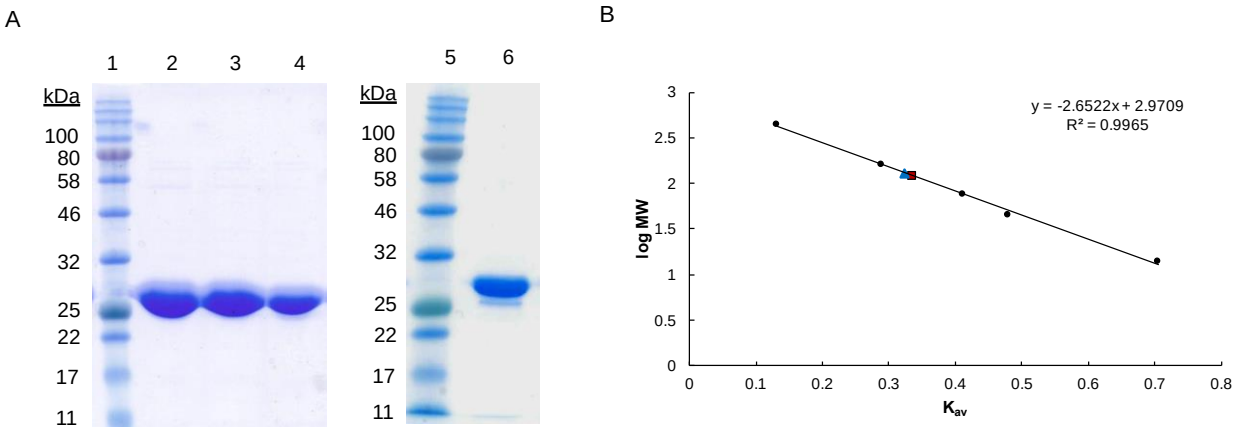

Figure S37. Steady-state kinetics of PtmO8 and PtmO1. Non-linear Michaelis-Menten regression plots of rate vs substrate concentrations were generated using GraphPad Prism 7 software (La Jolla, CA) to calculate the kinetic constants for each substrate. The determined kinetic parameters are summarized in Table 1 in the main text. Kinetics were performed in triplicate and each data point represents the mean of the three independent assays with error bars representing the standard deviation. (A) PtmO8 (200 nM) was incubated with varying concentrations (2–300 μM) of **6**. (B) PtmO8 (200 nM) was incubated with varying concentrations (2–300 μM) of **10**. (C) PtmO8 (200 nM) was incubated with varying concentrations (5–500 μM) of NAD^+. (D) PtmO8 (2 μM) was incubated with varying concentrations (0.02–3 mM) of $NADP^+$. (E) PtmO1 (20 nM) was incubated with varying concentrations (10–300 μM) of **7**. (F) PtmO1 (40 nM) was incubated with varying concentrations (0.5–200 μM) of **11.**

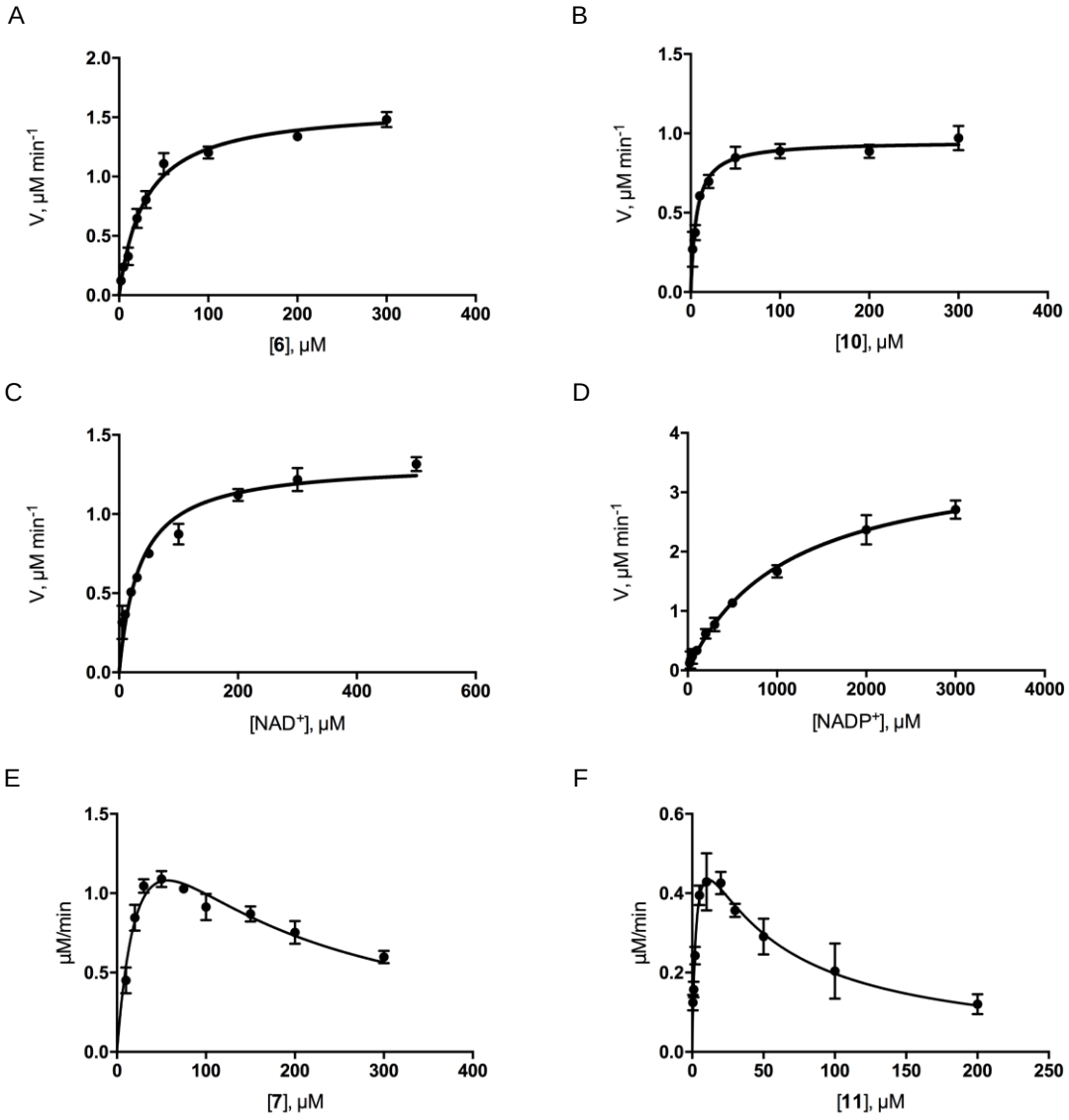

Figure S38. Homology models of PtmO8 and PtmO1. Homology models were constructed for PtmO8 (A/B) and PtmO1 (C/D) using the I-TASSER server,[15] giving C-scores of 0.88 and 0.92, respectively. The tetrameric structures (A/C) were based on the sepiapterin reductase crystal (PDB 2BD0),[28] and the native substrates for each, NAD^+ (PtmO1) and NADPH (PtmO8) were docked into their conserved binding sites. The expected charged residues (D37 in PtmO8; R41 in PtmO1) were located near where the phosphate of NADPH would be bound, providing evidence to support the cofactor selectivities of the two enzymes.

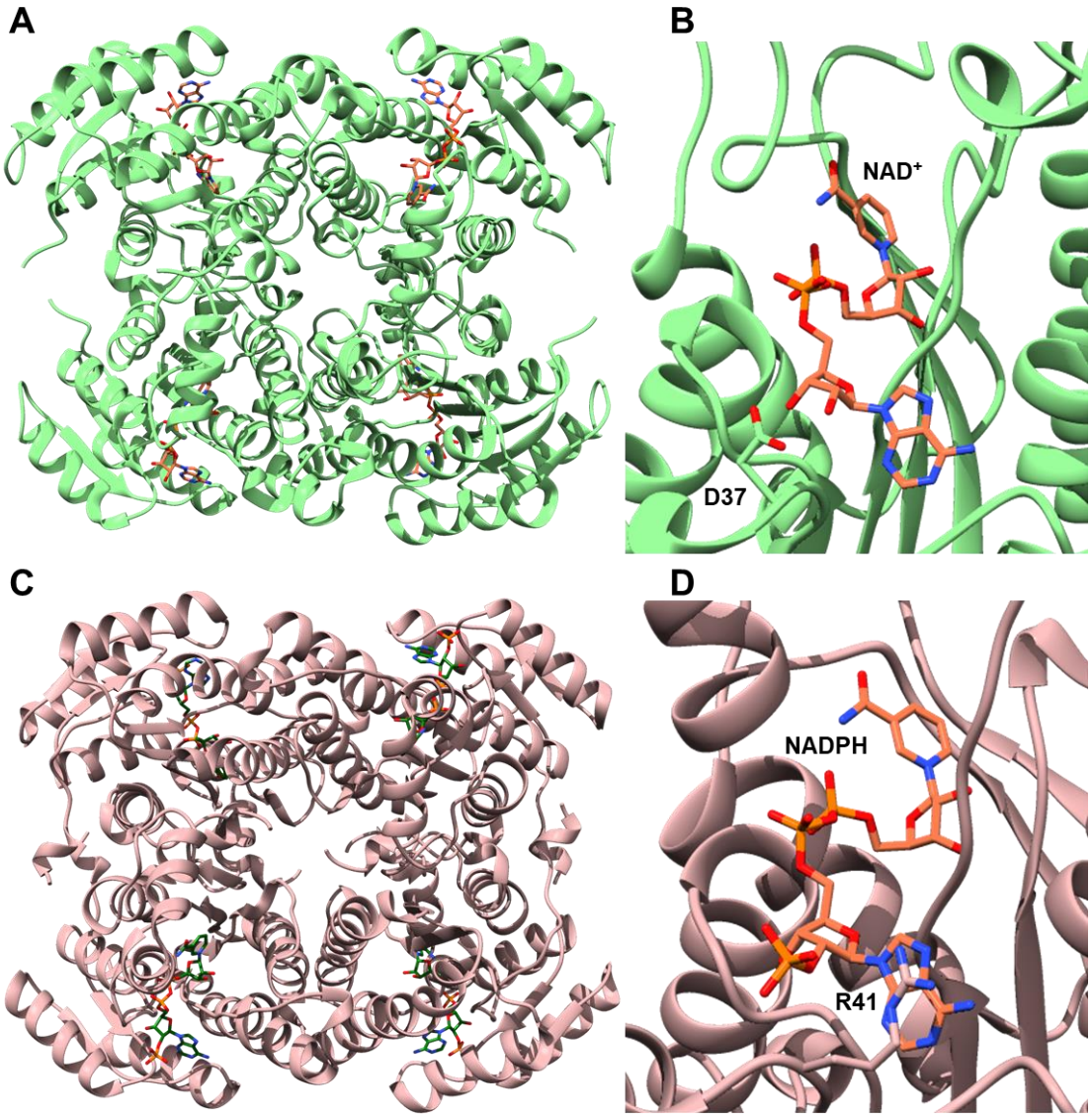

Figure S39. A plausible biosynthetic pathway to the enone in PTM and PTN biosynthesis. (A) The different reaction mechanism of the type I and II DHQase to the dehydroshikimate. Although type I and II DHQase catalyze the same overall reaction, they are different enzymes with distinct structures and mechanisms.[29] (B) A plausible biosynthetic pathway to the enone in PTM and PTN biosythesis. The C7 β-hydroxyl in **7-βOH** may hinder the C5 hydroxylation that was proposed initiating A-ring cleavage via a retro-aldol reaction.[25] The C7 α-hydroxyl may dehydrate via a *cis*-dehydration mechanism similar with the type I dehydroquinase in the shikimate pathway shown in (A). The enone product of PTM ML1 was previously isolated from SB12030 (*ΔptmO4*) mutant.[3]

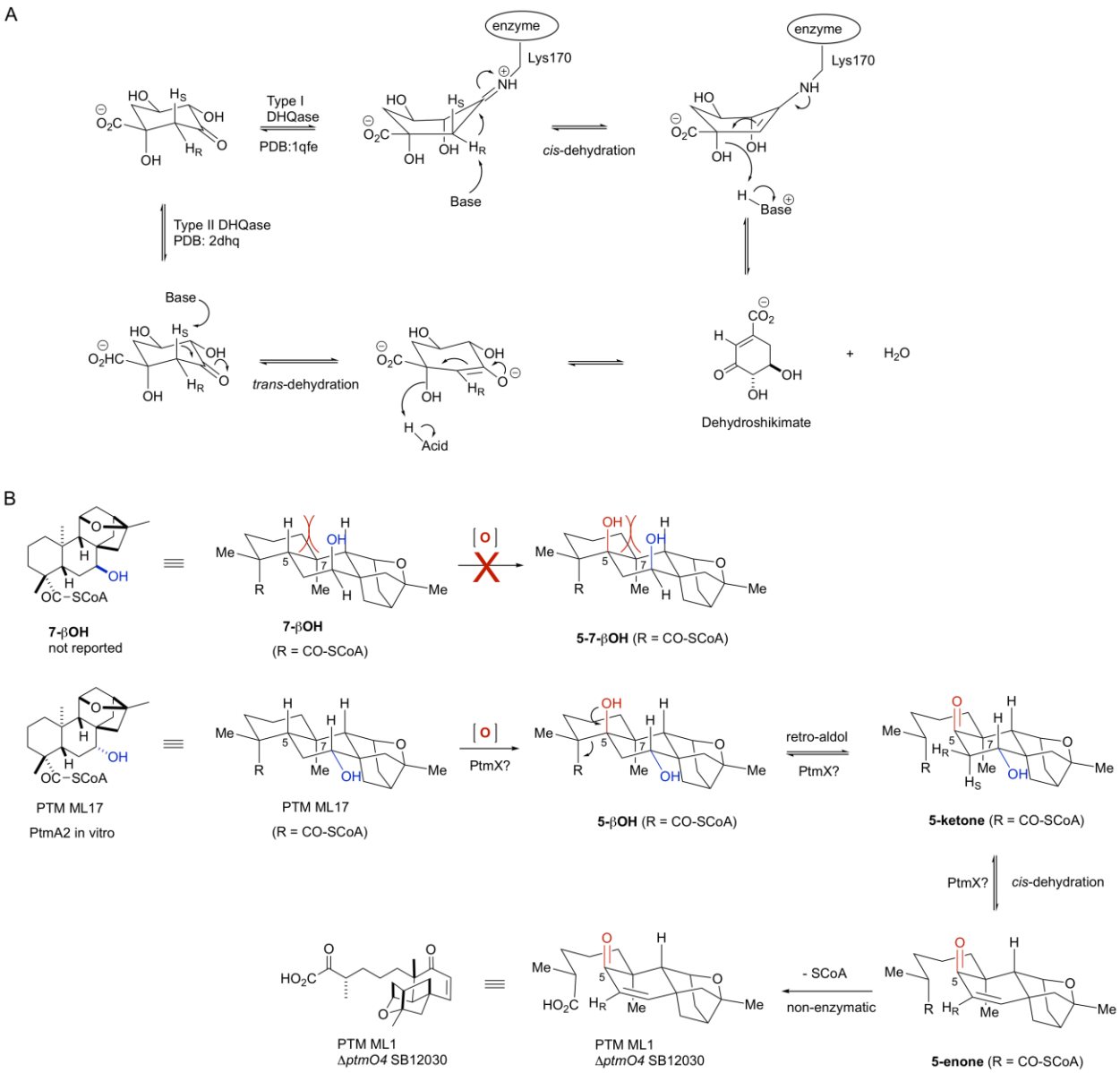

Supplementary References

1. Gust, B.; Challis, G. L.; Fowler, K.; Kieser, T.; Chater, K. F. PCR-targeted *Streptomyces* gene replacement identifies a protein domain needed for biosynthesis of the sesquiterpene soil odor geosmin. *Proc. Natl. Acad. Sci. U. S. A.* **2003,** *100*, 1541-1546.
2. MacNeil, D. J.; Gewain, K. M.; Ruby, C. L.; Dezeny, G.; Gibbons, P. H.; MacNeil, T. Analysis of *Streptomyces avermitilis* genes required for avermectin biosynthesis utilizing a novel integration vector. *Gene* **1992,** *111*, 61-8.
3. Rudolf, J. D.; Dong, L.-B.; Huang, T.; Shen, B. A genetically amenable platensimycin- and platencin-overproducer as a platform for biosynthetic explorations: a showcase of PtmO4, a long-chain acyl-CoA dehydrogenase. *Mol. BioSyst.* **2015,** *11*, 2717-2726.
4. Sheldrick, G. M. A short history of SHELX. *Acta Crystallogr., Sect. A: Found. Crystallogr.* **2008,** *64*, 112-122.
5. Wang, N.; Rudolf, J. D.; Dong, L.-B.; Osipiuk, J.; Hatzos-Skintges, C.; Endres, M.; Chang, C.-Y.; Babnigg, G.; Joachimiak, A.; Phillips, J. G. N.; Shen, B. Natural separation of the acyl-CoA ligase reaction results in a non-adenylating enzyme. *Nat. Chem. Biol.* **2018,** *14*, 730-737.
6. Cherepanov, P. P.; Wackernagel, W. Gene disruption in *Escherichia coli*: TcR and KmR cassettes with the option of FlP-catalyzed excision of the antibiotic-resistance determinant. *Gene* **1995,** *158*, 9-14.
7. Murakami, T.; Iida, H.; Tanaka, N.; Saiki, Y.; Chen, C.-M.; Iitaka, Y. Chemical and chemotaxonomic studies of ferns. XXXIII. Chemical studies on the constituents of *Pteris longipes* Don. *Chem. Pharm. Bull.* **1981,** *29*, 657-62.
8. Cherney, E. C.; Lopchuk, J. M.; Green, J. C.; Baran, P. S. A unified approach to *ent*-atisane diterpenes and related alkaloids: Synthesis of (-)-methyl atisenoate, (-)-isoatisine, and the hetidine skeleton. *J. Am. Chem. Soc.* **2014,** *136*, 12592-12595.
9. Lohman, J. R.; Bingman, C. A.; Phillips, G. N.; Shen, B. Structure of the bifunctional acyltransferase/decarboxylase LnmK from the leinamycin biosynthetic pathway revealing novel activity for a double-hot-dog fold. *Biochemistry* **2013,** *52*, 902-911.
10. Alves, J.; Vidugiris, G.; Goueli, S. A.; Zegzouti, H. Bioluminescent high-throughput succinate detection method for monitoring the activity of JMJC histone demethylases and Fe(II)/2-oxoglutarate-dependent dioxygenases. *SLAS Discovery* **2018,** *23*, 242-254.
11. Hindra; Huang, T.; Yang, D.; Rudolf, J. D.; Xie, P.; Xie, G.; Teng, Q.; Lohman, J. R.; Zhu, X.; Huang, Y.; Zhao, L.-X.; Jiang, Y.; Duan, Y.; Shen, B. Strain prioritization for natural product discovery by a high-throughput real-time PCR method. *J. Nat. Prod.* **2014,** *77*, 2296-2303.
12. Zhan, Z.-J.; Zhang, F.-Y.; Li, C.-P.; Shan, W.-G. A novel ent-kaurane diterpenoid from *Pteris semipinnata*. *J. Chem. Res.* **2009**, 149-150.
13. Pinar, M.; Rodriguez, B.; Alemany, A. Gummiferolic acid, a new ent-atis-16-ene diterpenoid from Margotia gummifera. *Phytochemistry* **1978,** *17*, 1637-40.
14. Fraga, B. M.; Gonzalez, P.; Gonzalez-Vallejo, V.; Guillermo, R.; Diaz, L. N. Biotransformation of 7α-hydroxy- and 7-oxo-ent-atis-16-ene derivatives by the fungus Gibberella fujikuroi. *Phytochemistry* **2010,** *71*, 1313-1321.
15. Roy, A.; Kucukural, A.; Zhang, Y. I-TASSER: a unified platform for automated protein structure and function prediction. *Nat. Protoc.* **2010,** *5*, 725-738.

16. Humphrey, W.; Dalke, A.; Schulten, K. VMD: visual molecular dynamics. *J Mol Graph* **1996**, *14*, 33-38.
17. Pettersen, E. F.; Goddard, T. D.; Huang, C. C.; Couch, G. S.; Greenblatt, D. M.; Meng, E. C.; Ferrin, T. E. UCSF Chimera-A visualization system for exploratory research and analysis. *J. Comput. Chem.* **2004**, *25*, 1605-1612.
18. Sanner, M. F.; Olson, A. J.; Spehner, J.-C. Reduced surface: an efficient way to compute molecular surfaces. *Biopolymers* **1996**, *38*, 305-320.
19. Nett, R. S.; Montanares, M.; Marcassa, A.; Lu, X.; Nagel, R.; Charles, T. C.; Hedden, P.; Rojas, M. C.; Peters, R. J. Elucidation of gibberellin biosynthesis in bacteria reveals convergent evolution. *Nat. Chem. Biol.* **2017**, *13*, 69-74.
20. Nett, R. S.; Dickschat, J. S.; Peters, R. J. Labeling studies clarify the committed step in bacterial gibberellin biosynthesis. *Org. Lett.* **2016**, *18*, 5974-5977.
21. Rojas, M. C.; Hedden, P.; Gaskin, P.; Tudzynski, B. The P450-1 gene of *Gibberella fujikuroi* encodes a multifunctional enzyme in gibberellin biosynthesis. *Proc. Natl. Acad. Sci. U. S. A.* **2001**, *98*, 5838-5843.
22. Helliwell, C. A.; Chandler, P. M.; Poole, A.; Dennis, E. S.; Peacock, W. J. The CYP88A cytochrome P450, *ent*-kaurenoic acid oxidase, catalyzes three steps of the gibberellin biosynthesis pathway. *Proc. Natl. Acad. Sci. U. S. A.* **2001**, *98*, 2065-2070.
23. Rudolf, J. D.; Dong, L.-B.; Manoogian, K.; Shen, B. Biosynthetic origin of the ether ring in platensimycin. *J. Am. Chem. Soc.* **2016**, *138*, 16711-16721.
24. Dong, L.-B.; Rudolf, J. D.; Shen, B. A mutasynthetic library of platensimycin and platencin analogues. *Org. Lett.* **2016**, *18*, 4606-4609.
25. Smanski, M. J.; Casper, J.; Peterson, R. M.; Yu, Z.; Rajski, S. R.; Shen, B. Expression of the platencin biosynthetic gene cluster in heterologous hosts yielding new platencin congeners. *J. Nat. Prod.* **2012**, *75*, 2158-2167.
26. Edgar, R. C. MUSCLE: multiple sequence alignment with high accuracy and high throughput. *Nucleic Acids Res.* **2004**, *32*, 1792-1797.
27. Robert, X.; Gouet, P. Deciphering key features in protein structures with the new ENDscript server. *Nucleic Acids Res.* **2014**, *42*, W320-W324.
28. Supangat, S.; Seo, K. H.; Choi, Y. K.; Park, Y. S.; Son, D.; Han, C.-d.; Lee, K. H. Structure of *Chlorobium tepidum* sepiapterin reductase complex reveals the novel substrate binding mode for stereospecific production of L-*threo*-tetrahydrobiopterin. *J. Biol. Chem*. **2006**, *281*, 2249-2256.
29. Gourley, D. G.; Shrive, A. K.; Polikarpov, I.; Krell, T.; Coggins, J. R.; Hawkins, A. R.; Isaacs, N. W.; Sawyer, L. The two types of 3-dehydroquinase have distinct structures but catalyze the same overall reaction. *Nat. Struct. Biol.* **1999**, *6*, 521-525.